



Development of water quality model in the Satilla River Estuary, Georgia

Lianyuan Zheng^{a,*}, Changsheng Chen^b, Frank Y. Zhang^c

^a College of Marine Science, University of South Florida, St. Petersburg, FL 33701, USA

^b School for Marine Sciences and Technology, University of Massachusetts-Dartmouth, New Bedford, MA 02744, USA

^c Department of Biology, Kean University, Union, NJ 07083, USA

Received 18 February 2003; received in revised form 18 December 2003; accepted 5 January 2004

Abstract

A coupled three-dimensional physical and water quality model was developed for the Satilla River Estuary, Georgia. The physical model is a modified ECOM-si version with inclusion of flooding/drainage process over the intertidal salt marsh. The water quality model is a modified WASP5 with inclusion of nutrient fluxes from the bottom sediment layer. The coupled model was driven by tidal forcings at the open boundary in the inner shelf of the South Atlantic Bight (SAB) and real-time river discharge at the upstream of the estuary. The initial condition for salinity was specified using the field measurement data taken along the estuary. The water quality components were assumed as constant values everywhere at the initial, with assumption that the spatial and temporal variations of these variables were caused by physical–biological–chemical interactions under strong tidal mixing environment. The model-predicted concentrations of inorganic nutrients (ammonium, nitrate plus nitrite, and ortho-phosphorus), chlorophyll-*a*, and dissolved oxygen (DO) in an along-estuary transect were in reasonable agreement with observational data. Process studies suggest that the intertidal salt marsh acts as a main sink for particulate materials and a major consumer of DO. The low DO concentration in the Satilla River Estuary was mainly due to high sediment oxygen demand (SOD) over the intertidal salt marsh. This feature is the nature of the estuarine–salt marsh ecosystem with nothing related to anthropogenic activities. Tidal mixing-induced bottom resuspension process played a critical role in supplying the nutrients in the water column in addition to the nitrification process. © 2004 Elsevier B.V. All rights reserved.

Keywords: Water quality; Satilla River Estuary; Bottom nutrient flux; Three-dimensional; Coupled physical and water quality model

1. Introduction

Estuaries, a mixing region between river and ocean waters, are the most valuable ecosystem related to human activity (Costanza et al., 1997). Excessive nutrient loadings from the land and atmospheric deposition, however, have become a serious environmental

issue in estuaries regarding the cause of unusual phytoplankton blooms and eutrophication. A national assessment of estuarine eutrophication conditions conducted in the US indicates that almost all estuaries exhibit some symptoms of eutrophication, though these symptoms vary widely in scale, intensity, and influence (Bricker et al., 1999). The temporal variability and spatial distributions of nutrients in estuaries are controlled by a complex physical–biological–chemical interaction process associated with external loading, tidal advection/dispersion, and wind mixing as well as groundwater inputs.

* Corresponding author. Tel.: +1 727 553 1639;
fax: +1 727 553 1189.
E-mail address: lzheng@seas.marine.usf.edu (L. Zheng).

Since these complicated processes are strong non-linearly coupled, studies of the nutrient-derived eutrophication usually rely on a water quality model with inclusion of inorganic and organic matter transformation and utilization. In addition to eutrophication, DO is the other critical variable in evaluating the water quality in estuaries. The low DO concentration in the water body directly affects survivals of fishes, migrations of higher organisms, and thus alters estuarine healthy ecological balance. Frequent occurrences of hypoxia due to sudden shutdown of DO have caused significant reduction of fishery harvests, toxic algal blooms, and loss of biotic diversity (Paerl, 1988; Howarth et al., 2000). The temporal variability and spatial variance of DO in estuaries are controlled by multiple physical and biochemical processes. Physical processes include current advection and turbulent mixing, while key biochemical processes are reaeration, oxidation due to the carbonaceous biochemical oxygen demand, phytoplankton photosynthesis and respiration, nitrification, sediment oxygen demand, and bacterial respiration (Ambrose et al., 1993; Chen, 2003). Since these physical and biochemical processes are non-linearly linked and are difficult to separate one from another from the field measurement or laboratory experiments, studies of DO are often conducted using a water quality.

The water quality has been extensively examined in many estuaries and lakes (James and Bierman, 1995; Wang et al., 1999; Cerco, 2000), but not in the Satilla River Estuary, Georgia. The Satilla River Estuary is characterized by extensive intertidal salt marshes, shallow water channel (about 4 m), and large tidal amplitudes (with a maximum value of 3 m during the spring tide). The large ratio of surface elevation to mean water depth makes the Satilla River Estuary a fully non-linear estuarine dynamic system. Previous field measurements revealed that the spatial and temporal variation of biological and chemical material is controlled by the semi-diurnal variability of tidal current (Windom et al., 1975; Pomeroy et al., 1993; Verity et al., 1993). During flood tidal phase, dissolved organic matter and particulate materials are transported onto intertidal salt marshes and deposited in the marshes. During ebb tidal phase, some deposited particulate materials are resuspended and carried into the estuarine channel. Observations also show that DO concentration in the Satilla River Estu-

ary decreases with the decrease of salinity as results of a large ratio of salt marsh to estuarine area (Winker et al., 1985). Sediment oxygen demand (SOD) is much higher in intertidal salt marshes than the main channel of the river, which directly attributes to the low DO measured in the marsh and in the upstream area of the river with extensive coverage of the marsh and low salinity water from freshwater outflow (Pomeroy et al., 2000).

Model results show that the current character in the main channel of the river depends on the water transport processes over the intertidal salt marshes. Eliminating this process leads to an approximately 5–10% overestimation of tidal amplitudes and 50% underestimation of the tidal current. Since the flooding/drying process plays an essential role in material exchange over the estuarine-intertidal salt marsh-tidal creek complex, studies of the water quality in the Satilla River Estuary must take this process into account.

The model-predicted residual currents in the Satilla River Estuary are featured by multiple eddy-like circulations. These residual eddies are formed as results of bottom topographic tidal rectification, inertial curvature coastal effects, along-estuarine baroclinic pressure gradient, and asymmetry of tidal current over flood and ebb phases. The existences of these eddies might act like retention zones to trap nutrients, plankton, and DO, thus leading these variables to patchy-like distributions. Due to a chaotic nature of water exchanges (Chen and Beardsley, 2002), however, retention mechanism might be broken down under the environment with periodic tidal forcing, and thus no permanent patchy structures could form for a long-term simulation.

Significant sediment resuspension was observed in the Satilla River Estuary (Blanton et al., 1999) and also reasonably captured in our model experiments (Zheng et al., 2003b). This suggests that the upward nutrient flux from the benthic sediment layer is active in this estuary, which might play an essential role in the nutrient balance in the water column. A remarkable along-estuarine variance was found in the model-predicted sediment resuspension, which was believed as results of the non-uniform distribution of the bottom stress and horizontal and cross-estuarine convergence and divergence of residual currents. If nutrients were distributed uniformly everywhere in the water column and benthic layer of the main channel

of the estuary at the initial, they would form patchy structures quickly over several tidal cycles as results of spatially non-uniform bottom fluxes and asymmetrically tidal mixing over flood and ebb tidal periods.

The objectives of this paper are to develop a coupled three-dimensional physical and water quality model for the Satilla River Estuary and use it to identify and quantify how the physical, biological, and chemical processes and their interactions control the spatial distributions of water quality components in the main channel of the river. This paper is organized as follows. In Section 2, the study area is described. In Section 3, field samplings and data synthesis are presented. In Section 4, the coupled physical and water quality model is given. In Section 5, model results are provided and discussed. Finally, in Section 6, conclusions are summarized.

2. Study area

The Satilla River Estuary, which has one of the largest areal extents of intertidal salt marshes in the US, is located in southeastern Georgia. This estuary is characterized by curved shoreline, with linkage to intensive intertidal salt marshes that are about three times as much as the main channel of the river (Fig. 1). The ratio of marsh area to estuarine area (defined as the estuarine focusing factor) gradually increases upstream. The width of the main channel of the river is approximately 4 km at the mouth and gradually narrows to about 1 km at the upstream end. The mean depth of the river is 4 m, with a maximum depth of 23 m near the mouth.

The Satilla River Estuary is a typical “blackwater” river characterized with high concentrations of humic and tannic acids, dissolved inorganic carbon and low PH (Beck et al., 1974; Dame et al., 2000). Freshwater discharge, originating from the upstream end over the coast plain, varies seasonally with a low rate of less than $10 \text{ m}^3 \text{ s}^{-1}$ during the fall and winter and a high rate of more than $1000 \text{ m}^3 \text{ s}^{-1}$ during the spring and summer. Tidal motion, dominated by the semi-diurnal M_2 tide, controls water movement of the Satilla River Estuary. M_2 tidal current can reach 100 cm s^{-1} , which accounts for about 80–90% of the along-estuary current variation (Blanton, 1996; Zheng et al., 2003a). Spring tidal variation accounts for 10–25% of total ki-

netic energy. Winds are northeasterly or northwesterly in winter and southeasterly or southwesterly in summer (Weber and Blanton, 1980).

3. Measurement results

In a US NSF-funded Land-Margin Ecosystem Research project in Georgia Rivers (LMER), two hydrographic cruises were conducted in the Satilla River Estuary in spring, 1995: the one on April 8 during the neap tide and the other on April 16 during the spring tide. Fig. 1 denotes the measurement stations extending from 0 to 36 km upstream from the mouth of the estuary. These surveys were made along a single along-estuary journey within 2 h around low and high waters, respectively. Water samples were collected about 1 m below the surface in the main channel by Niskin sampler or peristaltic pump and impeller, or bottles by Dr. William Wiebe and Joan Sheldon at the University of Georgia. The samples were frozen in acid-washed polyethylene bottles and transported to the lab where they were stored at -20°C or lower. Concentrations of dissolved ammonium and ammonia were measured by using Koroleff (1983)’s method, and the concentrations of dissolved nitrate and nitrite were measured by using the so-called “spongy cadmium” method (Jones, 1984). The concentration of dissolved inorganic phosphorus was measured by autoanalyzer (D’Elia et al., 1987), which was based on Technicon Industrial Method No. 155-71W. Under a 95% confidence level, the precision of measurements is 0.08, 0.3, and $0.05 \mu\text{M}$ for ammonium, nitrate, and ortho-phosphorus, respectively (Wiebe and Sheldon, personal communication). No chlorophyll-*a* concentration was directly measured during these two cruises, except un-calibrated fluorescence measurements made in April 1995 by Dr. Jack Blanton at the Skidaway Institute of Oceanography. The chlorophyll-*a* concentration was estimated inversely through a relationship between chlorophyll-*a* and fluorescence concentrations derived from later LMER cruises conducted in October 1996 and July 1997. The least square method was used to find the best fitting of these two data sets, which resulted in a square polynomial relationship with a correlation coefficient of $r^2 = 0.91$ as follows

$$\text{Chla} = -0.0283 f^2 + 2.5146 f - 14.224 \quad (1)$$

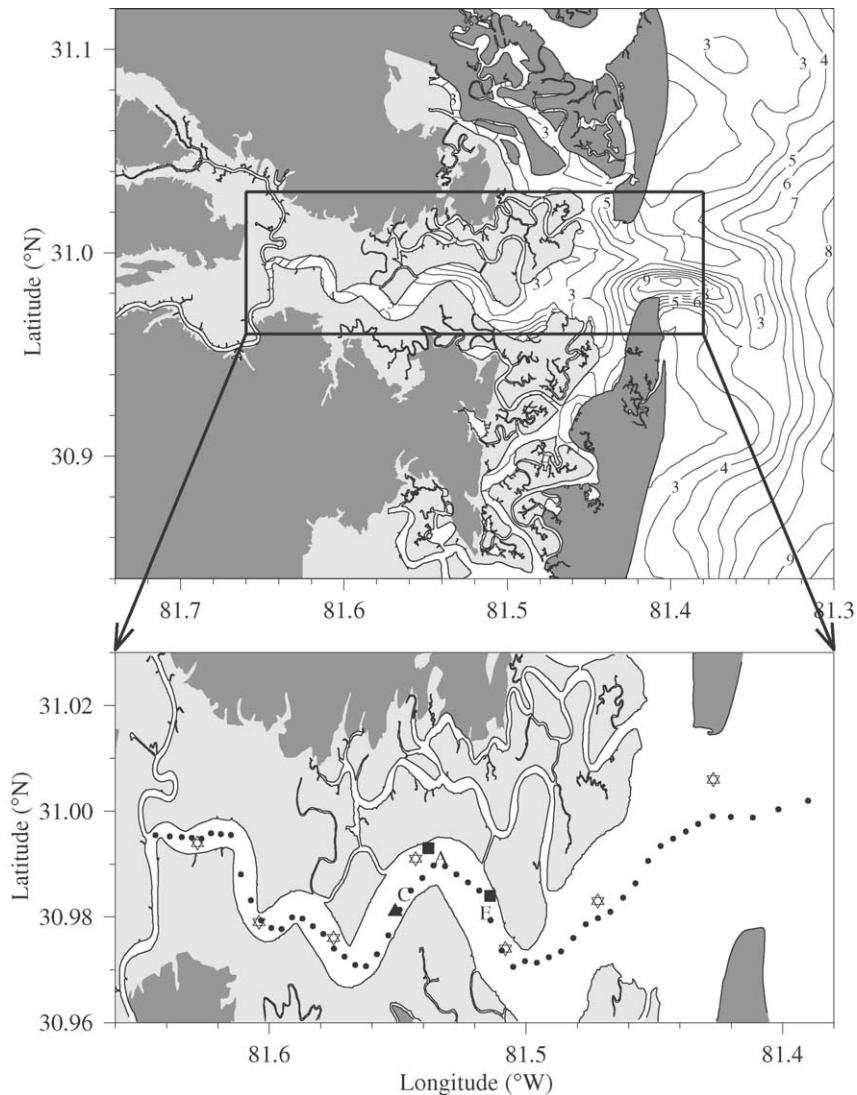


Fig. 1. Georgia coastline (upper) and location of the Satilla River Estuary (lower). The light gray filled area is the 2 m intertidal zone. Stars are the along-river CTD measurement stations taken on April 16, 1995. Filled squares (A and E) are the locations of the two current meter-mooring sites. The filled triangle (C) is the anchor site where a time series of CTD measurements was made. Filled circles are the selected along-estuary section. Water depth (m) is provided in the upper panel.

where Chl_a and f are chlorophyll-*a* and fluorescence concentrations, respectively. The concentration of the chlorophyll-*a* was measured by Dr. Merryl Alber at the University of Georgia. This estimation of chlorophyll-*a* concentrations was made based on an assumption that the relationship between chlorophyll-*a* and fluorescence concentrations would not change significantly with season.

The along-estuarine distribution of ammonium varied significantly with respect to spring-neap tidal cycles (Fig. 2a). During the spring tide, the near-surface concentration of ammonium observed in the along-estuary transect was lowest with values of less than $5 \mu\text{g N l}^{-1}$ near the estuary mouth, sharply increased to $50 \mu\text{g N l}^{-1}$ or higher at the mid-section of the estuary in a region with maxi-

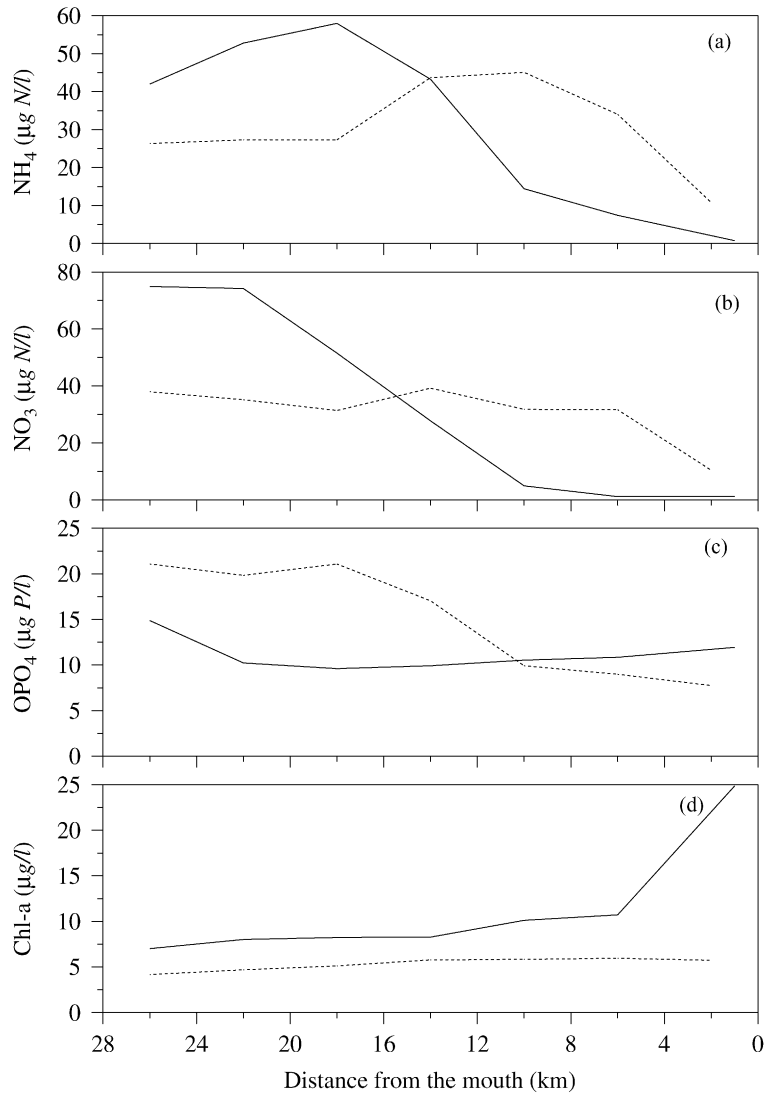


Fig. 2. Observed concentrations of ammonium (a), nitrate plus nitrite (b), ortho-phosphorus (c), and chlorophyll-*a* (d) along the estuary on April 7, 1995 during the neap tide (dashed line) and April 16, 1995 during the spring tide (solid line). The measurement sites are shown in Fig. 1. The ammonium, nitrate + nitrite and ortho-phosphorus were measured by Dr. W. Wiebe and J. Sheldon and the chlorophyll-*a* samples were collected and analyzed by Drs. M. Alber and J. Blanton.

num sediment resuspension and a salinity of 10 PSU (practical salinity unit) (Zheng et al., 2003a,b), and then gradually decreased to $40 \mu\text{g N l}^{-1}$ or lower close to the upstream end. This distribution pattern was the same as that observed in the Parker River in Massachusetts—a similar marsh-dominated estuary (Vörösmarty and Loder, 1994). During the neap tide, the concentration of ammonium was about $15 \mu\text{g}$

N l^{-1} near the estuary mouth, increased to $40 \mu\text{g N l}^{-1}$ at 10 km upstream, decreased to $25 \mu\text{g N l}^{-1}$ at 18 km upstream, and then remained constant to the upstream end. In the region between the mouth of the estuary and 14 km upstream, the concentration of ammonium is higher during the neap tide than during the spring tide, while it was inverted in the further upstream.

The distributions of the near-surface concentrations of nitrate + nitrite and inorganic phosphorus observed in the along-estuary transect significantly differed during spring and neap tides (Fig. 2b and c). During the spring tide, the concentrations of nitrate + nitrite monotonously increased from the mouth of the estuary to the upstream end, with a maximum value of $75 \mu\text{g N l}^{-1}$, and the concentration of inorganic phosphorus had a value of about $12 \mu\text{g P l}^{-1}$ near the mouth of the estuary and $14 \mu\text{g P l}^{-1}$ in a region close to the upstream end, with a minimum value of $9.5 \mu\text{g P l}^{-1}$ in the mid-segment of the estuary. During the neap tide, the concentration of nitrate + nitrite was higher in the segment between the estuary mouth and 15 km upstream but was lower in the further upstream region, and the concentration of inorganic phosphorus monotonously increased upstream-ward. That fact that nitrate + nitrite was high and ammonium was low in a region close to the upstream end suggested a high nitrification rate in the relatively fresher and high turbid water. This was consistent with the findings in the Mississippi and Atchafalaya Rivers by Pakulski et al. (2000).

The distribution of the near-surface chlorophyll-*a* concentration observed in the along-estuary transect also showed significant patterns during spring and neap tides (Fig. 2d). During the spring tide, it had a maximum value of $25 \mu\text{g l}^{-1}$ near the mouth of the estuary, decreased sharply to about $10 \mu\text{g l}^{-1}$ at the location 6 km upstream, and then decreased gradually to $8 \mu\text{g l}^{-1}$ in a region close to the upstream end. During the neap tide, the concentration of chlorophyll-*a* exhibited a relatively stable value of about $5 \mu\text{g l}^{-1}$ everywhere in the main channel of the estuary. The low chlorophyll-*a* concentration inside the estuary was likely related to high turbidity, since turbidity reduced light penetration in water column and decreased phytoplankton productivity.

4. The coupled physical and water quality model

4.1. Physical model

The physical model used in this study was a fully three-dimensional estuarine and coastal ocean model (ECOM-si) developed originally by Blumberg (1993). It incorporates the Mellor and Yamada (1982) level

2.5 turbulent closure sub-model, with modification by Galperin et al. (1988) to provide realistic vertical turbulent mixing parameters. A semi-implicit finite difference scheme was used, by which the advection, Coriolis, baroclinic pressure gradient, and horizontal diffusion terms were calculated by an explicit scheme, and the barotropic pressure gradient (or surface elevation gradient) and vertical diffusion terms were solved implicitly. Three advantages of the semi-implicit finite difference scheme are (1) generating a symmetric, positive definite system for surface elevation, which can be effectively solved by a preconditioned conjugate gradient method (Casulli, 1990); (2) allowing us to use the same time step for internal and external modes; and (3) removing external Courant–Friedrichs–Levy (CFL) constraint. Although the semi-implicit scheme used in ECOM-si may damp the energy of the surface wave, it showed no significant influences on the short-time simulation in strong tidal mixing Satilla River Estuary.

The ECOM-si was modified by Zheng et al. (2003a,b) to add a wet/dry treatment technique for the study of water flushing onto and draining from the intertidal salt marsh during the tidal cycle and by Chen and Beardsley (1998) to add a multidimensional positive definite advection transport algorithm (MPDATA) (Smolarkiewicz, 1984) for non-linear advection terms in the salinity transport equation. To avoid a singularity problem, a viscous boundary layer with a thickness of h_c was added into the water depth. Total depth was redefined as the sum of $H(x, y)$ (reference water depth), $\zeta(x, y, t)$ (surface elevation), and h_c . The grid was treated as a wet point if D was larger than h_c , otherwise it remained a dry point. By introducing an “anti-diffusion” velocity to the successive application of an upwind scheme with correction to the first-order truncation error, MPDATA yielded a positive definite and second-order accurate advection algorithm. The modified model has been applied to a simulation of temporal and spatial distributions of the three-dimensional tidal current and salinity in the Satilla River Estuary. A comparison of model results was made between the cases with and without inclusion of the flooding/drying process, suggesting that the flooding/drying process accounted for about 40–50% water transport in the estuary. The model results were also evaluated by direct comparison with observed tidal elevation, tidal currents and salinity. A

detailed description of the model performance was given by Zheng et al. (2003a).

4.2. Water quality model

The water quality model used in this study was built based on three-dimensional conventional water quality analysis simulation program (called WASP5) developed originally by Ambrose et al. (1993). It constitutes a complex of four interacting systems: dissolved oxygen, nitrogen cycle, phosphorus cycle, and phytoplankton dynamics. Eight water quality components are included: dissolved oxygen (DO), phytoplankton as carbon (PHYT), carbonaceous biochemical oxygen demand (CBOD), ammonium nitrogen (NH₄), nitrate and nitrite nitrogen (NO₃), ortho-phosphorus or inorganic phosphorus (OPO₄), organic nitrogen (ON), and organic phosphorus (OP). The conceptual framework for the water quality model is presented in Fig. 3.

A mathematical formulation of the conservation of mass can be written as:

$$\begin{aligned} \frac{\partial C}{\partial t} + \frac{\partial(uC)}{\partial x} + \frac{\partial(vC)}{\partial y} + \frac{\partial(wC)}{\partial z} \\ = \frac{\partial}{\partial x} \left(A_h \frac{\partial C}{\partial x} \right) + \frac{\partial}{\partial y} \left(A_h \frac{\partial C}{\partial y} \right) \\ + \frac{\partial}{\partial z} \left(K_h \frac{\partial C}{\partial z} \right) + S + W_0 \end{aligned} \quad (2)$$

where *C* is the concentration of the water quality components; *u*, *v*, and *w* are the water velocity components corresponding to the conventional Cartesian coordinate system (*x*, *y*, *z*); *A_h* and *K_h* are the coefficients of the horizontal viscosity and vertical eddy diffusion, respectively; *S* is the function that represents the internal source or sink of the water quality component (see Appendix A); and *W₀* is the external loading from point (river discharge) and non-point sources (ground-

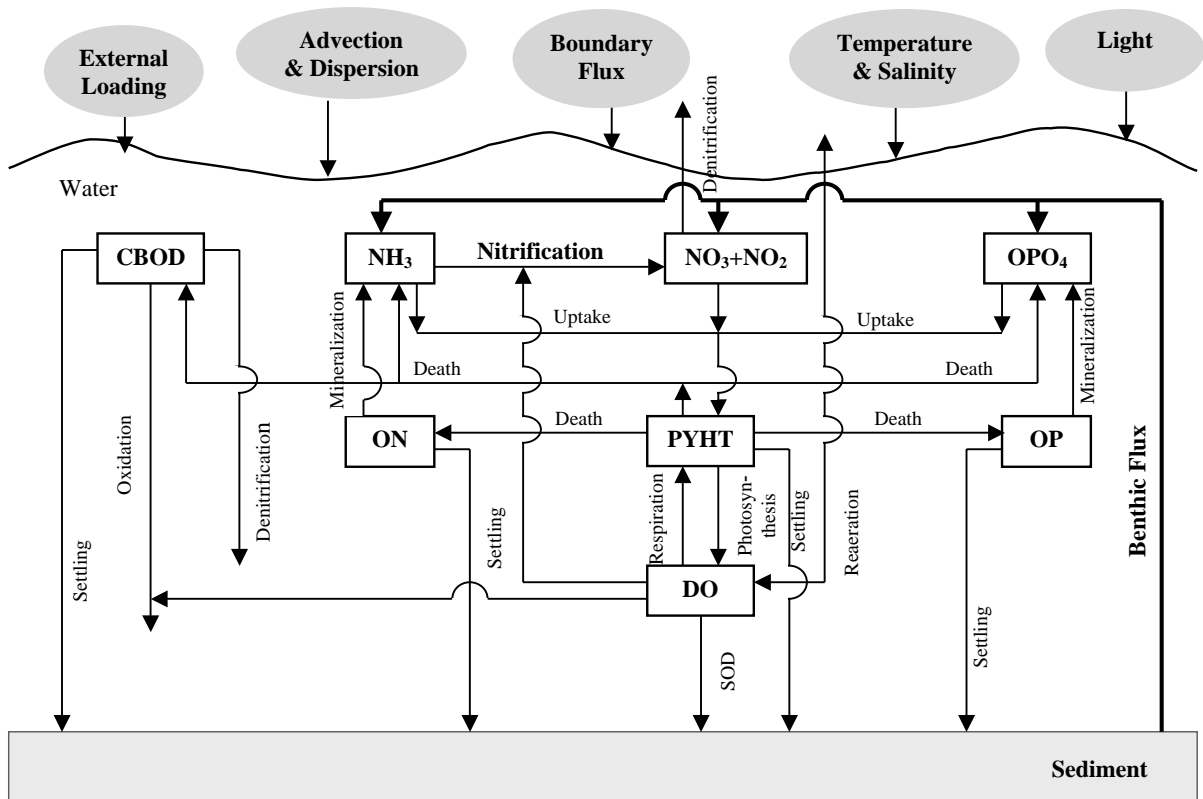


Fig. 3. Schematic of water quality model used for the Satilla River Estuary.

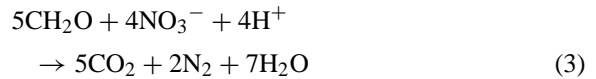
water input and atmospheric deposition) of the water quality components.

Dissolved oxygen is one of the most important water quality indicators. One source for DO in the water column is photosynthesis carbon fixation. It is proportional to phytoplankton density and growth rate. Wind- or flow-induced reaeration can be either the source or sink for DO. If DO concentration in the water column is under-saturation, reaeration will act as a source for DO. Otherwise, reaeration is a sink for DO. Dissolved oxygen in the water column is diminished by the processes associated with SOD, phytoplankton respiration, nitrification, and oxidation of CBOD (Fig. 3).

The growth rate of phytoplankton is the function of solar radiation, water temperature, nutrient availability, and euphotic depth. The effect of nutrients on growth rate is assumed to follow the Michaelis–Menten function (Monod, 1949), which indicates that phytoplankton growth rate is linearly proportional to nutrient at a low level of the concentration but is independent of nutrient at a high level of the concentration. The light-limiting factor used here was developed by Di Toro et al. (1971). It shows that growth rate only occurs in the euphotic zone and increases as a function of light intensity until an optimum intensity is reached.

The productivity of phytoplankton is affected by endogenous respiration, effect of viral lysis, grazing by zooplankton, and settling to bottom sediment layer. Zooplankton grazing may play an important role in phytoplankton productivity in the estuarine system. Detailed specifications of zooplankton predation are required for predictive modelling of planktonic biomass and their interaction. Instead of being attempt to model the complex and dynamic processes of zooplankton grazing and growth, a constant grazing rate is assumed in the model.

The primary internal source of CBOD comes from the detrital phytoplankton carbon as a result of death of primary producers, such as phytoplankton and benthic algae, and zooplankton predation. The internal sinks for CBOD include carbonaceous oxidation and settling of particulate carbonaceous material to bottom sediment. When the DO concentration in the water body is low, the denitrification reaction also provides a sink for CBOD by following reaction:



In the nitrogen cycle, ammonium nitrogen, nitrate and nitrite (hereafter called nitrate) nitrogen, and organic nitrogen are included. During phytoplankton growth, they directly uptake inorganic ammonium and nitrate nitrogen, while when phytoplankton respire or die due to zooplankton predation, they return a certain fraction to the organic nitrogen pool and the other to inorganic ammonium nitrogen pool. In the presence of DO, the ammonium nitrogen can be converted to nitrate nitrogen (called nitrification). This process is affected by pH, flow condition, salinity, and turbidity (Pakulski et al., 2000; Dr. S. Joye, University of Georgia, personal communication). Under low DO condition, nitrate nitrogen can be converted to dinitrogen (called denitrification). In the organic nitrogen pool, its particulate fraction will settle and deposit on the bottom sediment when the water body is calm. Also the organic nitrogen can be converted to ammonium nitrogen by bacterial decomposition or mineralization before it can be taken up by phytoplankton.

Previous study indicates that there is a large amount of particulate organic material inputs from intertidal salt marsh into the Satilla River Estuary (Pomeroy and Wiegert, 1981). The majority of these organic materials is deposited and buried on the bottom sediment layer. Excess particulate organic nitrogen in the sediment layer is then mineralized to inorganic ammonium nitrogen by heterotrophic bacterial activity. Further, through nitrification, some ammonium nitrogen in the sediment layer can be converted to nitrate nitrogen. As a result, there might be a large ammonium and nitrate nitrogen pool within the bottom sediment. When bottom current is strong enough to erode and resuspend sediment, it will transport nutrients from the sediment layer into upper water column by vertical mixing. In addition, when there is a nutrient concentration gradient between the water column and sediment layer, there will be nutrient flux between them by diffusion. The above statements imply that nutrient flux from the bottom sediment layer might be a potentially important nutrient source in the Satilla River Estuary. The importance of benthic nutrient flux has been reported in lakes (James et al., 1997), bays (Giblin et al., 1997), and estuary (Cowan and Boynton, 1996; Cowan et al., 1996; Kemp et al., 1997; Wang et al., 1999).

In the phosphorus cycle, ortho-phosphorus and organic phosphorus are included. Two internal sources of inorganic phosphorus are (1) recycled directly from phytoplankton respiration and death, and (2) converted from organic phosphorus via mineralization or bacterial decomposition. The ortho-phosphorus is consumed by phytoplankton uptake. The main source of organic phosphorus is recycled from phytoplankton respiration and death. Under calm condition, particulate organic phosphorus will sink and deposit on the bottom sediment layer. Like the nitrogen cycle, ortho-phosphorus flux from the bottom sediment layer might be an important source in the system.

The water quality equations are solved using the same finite difference method used in ECOM-si. To avoid negative concentrations and artificial numerical diffusion, the advection terms are calculated by using the MPDATA scheme. Horizontal and vertical diffusion terms are solved by explicit and implicit schemes, respectively.

4.3. Design of model experiments

Fig. 4 presents the overall view of the computational grid used in this study. The open boundary is located in the inner shelf of SAB, 20 km away from the mouth of the Satilla River Estuary. The horizontal grids are designed using an orthogonal curvilinear coordinate with a total of 148 (along-river) \times 141 (cross-river) points, resulting in grid resolution ranging from 100 m in the main estuarine channel and intertidal zones and to about 2.5 km close to the open boundary. Eleven σ -levels are uniformly distributed in the vertical to smoothly represent irregular bottom topography. This corresponds to a vertical resolution of less than 2.2 m at the 23 m depth (the deepest depth of the computational domain) and 0.2–0.5 m in the main estuarine channel. The time step in all the model runs is 41.4 s, 1080 time steps over an M_2 tidal cycle.

The physical model is initially driven by the M_2 , S_2 , and N_2 tidal elevations and phases at the open boundary. The model was first run for 60 M_2 tidal cycles to assure reaching an equilibrium state. It was continuously run to the point that the model-predicted tidal elevation reached the low water of the neap tide. Then the salinity distribution was specified using the CTD measurement data taken on April 7, 1995 and the real-time freshwater discharge was introduced

into the model domain at the upstream end of the estuary.

To simplify the water quality model experiments, the following assumptions were made. First, feedback effects of water quality components on water density were ignored. This allowed us to easily couple the water quality with the physical model without modifying estuarine circulation and water density. Second, since there were not enough observations regarding organic material input from salt marsh and the contribution of primary producers from the salt marsh, we ignored external loading to the estuary from the salt marsh. Third, once the particulate organic nitrogen, organic phosphorus, CBOD, and phytoplankton sank and deposited in the bottom, they were no longer considered in the model. This assumption indicates that no resuspension of these particulate materials from the bottom sediment layer occurs, although bottom stress is stronger than critical stress for sediment resuspension.

The water quality model experiments started at the low water on April 7, 1995 during the neap tide and ran for 9 days, after which model-predicted results of water quality components were output to compare with observations taken on April 16, 1995 during the spring tide. To test our hypothesis that the spatial variations of water quality components in the Satilla River Estuary were mainly controlled by physical and internal biogeochemical processes, the initial distributions of water quality components were assumed to be uniform in space and their values are provided in Table 1. These values were based on observations conducted in this estuary (DO, PHYT, NH_4 , NO_3 , and OPO_4) or in the Chesapeake Bay (CBOD, ON, and OP) (Shen, 1996).

4.4. Parameters used in water quality model

The water quality model includes 51 parameters. These parameters are specified based on observations

Table 1
The initial concentrations of water quality components

Variable (unit)	Value	Variable (unit)	Value
DO ($mg\ O_2\ l^{-1}$)	8.0	NO_3 ($mg\ N\ l^{-1}$)	0.04
CBOD ($mg\ C\ l^{-1}$)	1.5	ON ($mg\ N\ l^{-1}$)	0.3
PHYT ($mg\ C\ l^{-1}$)	0.3	OPO_4 ($mg\ P\ l^{-1}$)	0.015
NH_4 ($mg\ N\ l^{-1}$)	0.02	OP ($mg\ P\ l^{-1}$)	0.01

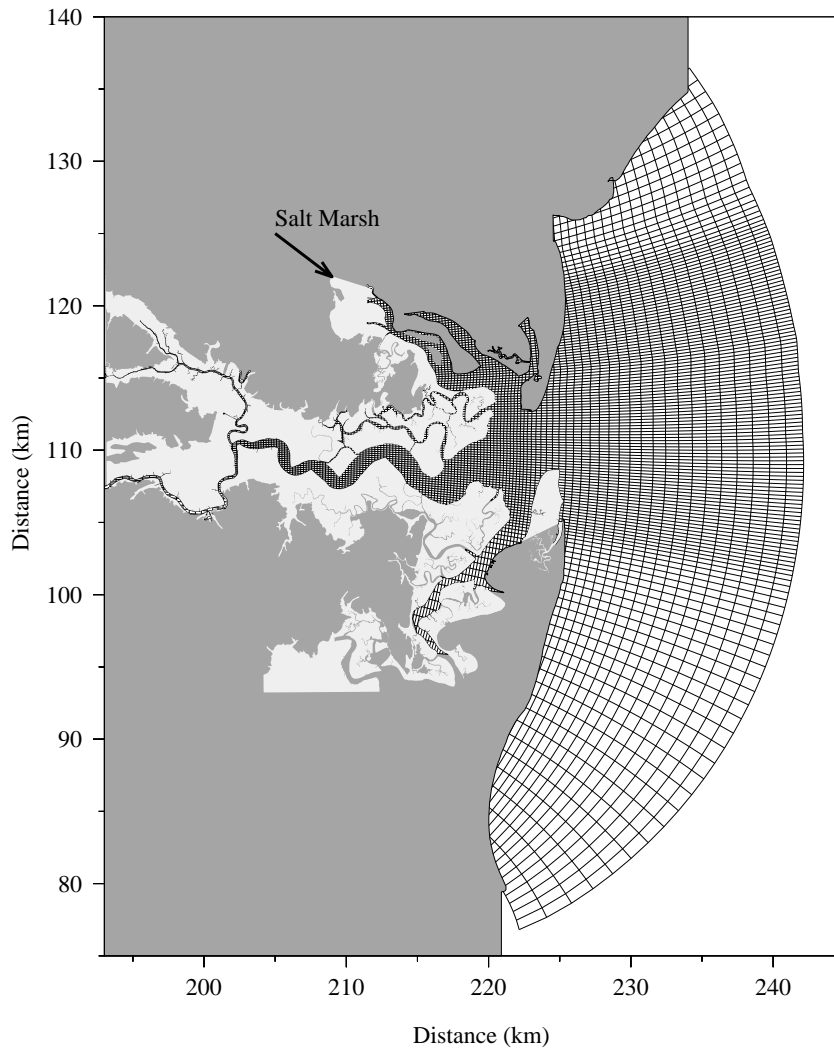


Fig. 4. The numerical computational grid. The light gray filled area is the 2-meter intertidal zone that can be reached during slack high water. The numerical domain consisted of 148 (along-river) \times 141 (cross-river) \times 11 (vertical) grid points. The horizontal resolution was 100 m in the main river channel and intertidal zone and gradually increased to 2.5 km over the inner shelf.

taken in the Satilla River Estuary and in other estuaries, or literature (Table 2). Observations revealed that sediment oxygen demand in the intertidal salt marsh was higher than in the estuary bed (Pomeroy et al., 1972). In the model experiment, SOD was specified as $2.5 \text{ g O}_2 \text{ m}^{-2} \text{ day}^{-1}$ in the inter-tidal salt marsh and $1.2 \text{ g O}_2 \text{ m}^{-2} \text{ day}^{-1}$ in the estuary bed. The light attenuation coefficient was given as 10 m^{-1} at the upstream end of the estuary and linearly decreased to 1.6 m^{-1} at the inner shelf, which corresponds to a light penetration depth of 10 cm at the upstream end of the es-

tuary and 60 cm at the inner shelf. Nitrification rates was found to be high in regions with low salinity and high turbidity (Pakulski et al., 2000). For simplification, we specified nitrification rate in the model as a function of salinity as follows:

$$k_{\text{ni}} = \begin{cases} 0.35 & S \leq 5 \\ \frac{0.35 - 0.25(15 - S)}{10.0} & 5 < S < 15 \\ 0.10 & S \geq 15 \end{cases} \quad (4)$$

Table 2
Parameters and constants for the water quality model

Name	Description	Units	Value
k_{r1}	Reaeration rate	Day ⁻¹	max(k_r , k_w) ^a
k_f	Flow-induced reaeration rate	Day ⁻¹	Covar method ^b
k_w	Wind-induced reaeration rate	Day ⁻¹	O'Connor method ^c
k_{d1}	CBOD deoxygenation rate	Day ⁻¹	0.20 ^a
k_{ni}	Nitrification rate	Day ⁻¹	Eq. (3)
k_{r2}	Phytoplankton respiration rate	Day ⁻¹	0.10 ^{a, d}
k_{r3}	Bacterial respiration rate	mg O ₂ day ⁻¹	0.20 ^d
k_{dn}	Denitrification rate	Day ⁻¹	0.09 ^a
k_{gr}	Phytoplankton optimum growth rate	Day ⁻¹	2.5 ^e
$k_{par} + k_{grz}$	Phytoplankton basal loss rate	Day ⁻¹	0.04 ^a
k_{m1}	Organic nitrogen mineralization rate	Day ⁻¹	0.075 ^a
k_{m2}	Organic phosphorus mineralization rate	Day ⁻¹	0.22 ^a
θ_{r1}	Temperature adjustment for reaeration rate	Unitless	1.028 ^a
θ_{d1}	Temperature adjustment for deoxygenation rate	Unitless	1.047 ^a
θ_{ni}	Temperature adjustment for nitrification rate	Unitless	1.080 ^a
θ_{r2}	Temperature adjustment for phytoplankton respiration rate	Unitless	1.080 ^a
θ_{dn}	Temperature adjustment for denitrification rate	Unitless	1.080 ^a
θ_{gr}	Temperature adjustment for phytoplankton growth rate	Unitless	1.066 ^a
θ_{mr}	Temperature adjustment for phytoplankton death rate	Unitless	1.000 ^a
θ_{m1}	Temperature adjustment for organic nitrogen mineralization rate	Unitless	1.080 ^a
θ_{m2}	Temperature adjustment for organic phosphorus mineralization rate	Unitless	1.080 ^a
θ_{SOD}	Temperature adjustment for SOD	Unitless	1.080 ^a
C_s	Dissolved oxygen saturation concentration	mg O ₂ l ⁻¹	Eq. (A.9) ^f
G_P	Phytoplankton growth rate	Day ⁻¹	Eq. (A.10) ^a
D_P	Phytoplankton death rate	Day ⁻¹	Eq. (A.11) ^a
P_{NH4}	Ammonium preference factor	Unitless	Eq. (A.12) ^a
SOD	Sediment oxygen demand	g m ⁻² day ⁻¹	1.2–2.5 ^{a, d}
K_{BOD}	Half-saturation concentration for oxygen limitation of CBOD oxidation	mg O ₂ l ⁻¹	0.5 ^a
K_{NITR}	Half-saturation concentration for oxygen limitation of nitrification	mg O ₂ l ⁻¹	0.5 ^a
K_{NO3}	Half-saturation concentration for oxygen limitation of denitrification	mg O ₂ l ⁻¹	0.1 ^a
K_{mN}	Half-saturation concentration for nitrogen uptake	μg N l ⁻¹	25.0 ^a
K_{mP}	Half-saturation concentration for phosphorus uptake	μg P l ⁻¹	1.0 ^a
K_{mPc}	Half-saturation concentration for phytoplankton limitation	mg C l ⁻¹	1.0 ^a
w_{2S}	Settling velocity of PHYT	m s ⁻¹	0.5 ^{a, g}
w_{2S}	Settling velocity of CBOD	m s ⁻¹	0.5 ^{a, g}
w_{2S}	Settling velocity of particulate organic nitrogen	m s ⁻¹	0.5 ^{a, g}
w_{2S}	Settling velocity of particulate organic phosphorus	m s ⁻¹	0.5 ^{a, g}
f_{D3}	Fraction of dissolved CBOD	Unitless	0.5 ^a
f_{D7}	Fraction of dissolved organic nitrogen	Unitless	1.0 ^a
f_{D8}	Fraction of dissolved organic phosphorus	Unitless	1.0 ^a
f_{on}	Fraction of dead and respired phytoplankton recycled to organic nitrogen pool	Unitless	0.65 ^e
f_{op}	Fraction of dead and respired phytoplankton recycled to organic phosphorus pool	Unitless	0.65 ^e
a_{nc}	Phytoplankton nitrogen–carbon ratio	Unitless	0.25 ^a
a_{pc}	Phytoplankton phosphorus–carbon ratio	Unitless	0.025 ^a
a_{oc}	Ratio of oxygen to carbon	Unitless	32/12 ^a
k_e	Light attenuation coefficient	m ⁻¹	1.0 ^g
B_1	Bottom ammonium flux	mg N day ⁻¹	Eq. (4)
B_2	Bottom nitrate flux	mg N day ⁻¹	Eq. (4)
B_3	Bottom ortho-phosphorus flux	mg P day ⁻¹	Eq. (4)
I_s	Optimal light intensity	ly day ⁻¹	250.0 ^g
D	Depth of benthic layer	m	0.5 ^g

^a Ambrose et al. (1993).^b Covar (1976).^c O'Connor (1983).^d Pomeroy et al. (2000).^e Yassuda et al. (2000).^f APHA (1985).^g Satilla River Estuary.

The fluxes of ammonium, nitrate and inorganic phosphorus (B_i , $i = 1, 2, 3$) from the bottom sediment layer were specified as being linearly proportional to the difference between model-predicted bottom stress and critical shear stress for settleable sediment resuspension:

$$B_i = c_i(\tau_b - \tau_{ce})^+ \quad (5)$$

where τ_b is the model-predicted bottom stress; τ_{ce} is the critical shear stress required for settleable sediment resuspension, which is specified as $0.196 \text{ kg s}^{-1} \text{ m}^{-2}$ (Blake et al., 2001) in this study; the superscript (+) is as an indicator of Heaviside's operator; c_1 , c_2 , and c_3 are the constant values specified as 0.2, 0.18, and 0.02, respectively. These values were determined by providing the best fit between observational data and model-predicted nutrient values during April 1995. In the model experiment, we assumed that there were an infinite nutrient source for ammonium nitrogen, nitrate nitrogen, and inorganic phosphorus in the bottom sediment layer. This means that as long as model-predicted bottom stress was larger than the critical stress, a net nutrient flux occurred at the bottom into the water column. This model experiment was referred as the standard run.

To examine the impacts of physical and biogeochemical processes on the distributions of water quality components, four additional sensitivity analysis experimental runs were conducted. In the first case, we removed the flooding/drying process over the intertidal salt marsh, i.e., no water was allowed to flood onto the intertidal salt marsh during the flood tidal phase. This experimental run was used to quantitatively examine the contribution of high SOD over intertidal salt marsh in DO depletion, and the impact of the flooding/drying process over the intertidal salt marsh on nutrient levels in the Satilla River Estuary. In the second experimental run, we eliminated nutrient flux from the bottom sediment layer. We specified a spatially and temporally constant salinity value of 35 PSU in the third experimental run to investigate the importance of salinity variation on the distributions of the water quality components. In the fourth experimental run, we ignored heterotrophic bacterial respiration to assess the contribution of bacterial respiration on DO concentration. All these runs were conducted using April 1995 conditions and the results

were compared with those predicted from the standard run.

5. Model results and discussions

5.1. Physical model

The model-predicted tidal elevation and currents were compared directly with the observed tidal elevations and currents at five bottom pressure measurement stations and two current meter sites in the Satilla River Estuary, respectively (Figs. 5 and 6). The results indicate that for M_2 , S_2 , and N_2 tidal constituents, the maximum differences of model-predicted and observed tidal elevations were less than 2.0 cm in amplitude and 10° in phase, and the maximum differences of model-predicted and observed tidal currents were less than 4 cm s^{-1} in major axis, 9° in orientation, and 25 min in phase. Good agreements were also found for salinity in the along-estuarine distribution and temporal variation at an anchor site measured on April 16, 1995 during the spring tide (Fig. 7). The model-data comparisons suggest that our physical model provided a reasonable simulation of the temporal and spatial distributions of the 3-D tidal current, salinity, and water exchange between estuarine channel and intertidal salt marsh in the Satilla River Estuary. A detailed description of tidal currents, residual circulation, and salinity was given in Zheng et al. (2003a).

5.2. Water quality model

In the standard experiment run (the initial concentrations and selected parameters are listed in Tables 1 and 2), the synoptic distributions of the model-predicted near-surface DO concentration at slack high water (SHW) and slack low water (SLW) on April 16, 1995 are presented in Fig. 8. DO concentration was high-spatially variable, which was highest with a value of more than $7 \text{ mg O}_2 \text{ l}^{-1}$ in the inner shelf and mouth of the estuary and decreased to less than $4 \text{ mg O}_2 \text{ l}^{-1}$ in the upstream end of the estuary. This spatial pattern was associated with differences in photosynthesis, nitrification, and SOD between the mouth of the estuary and upstream region of the estuary. Compared with the inner shelf and mouth of the estuary, turbidity inside the estuary was relatively

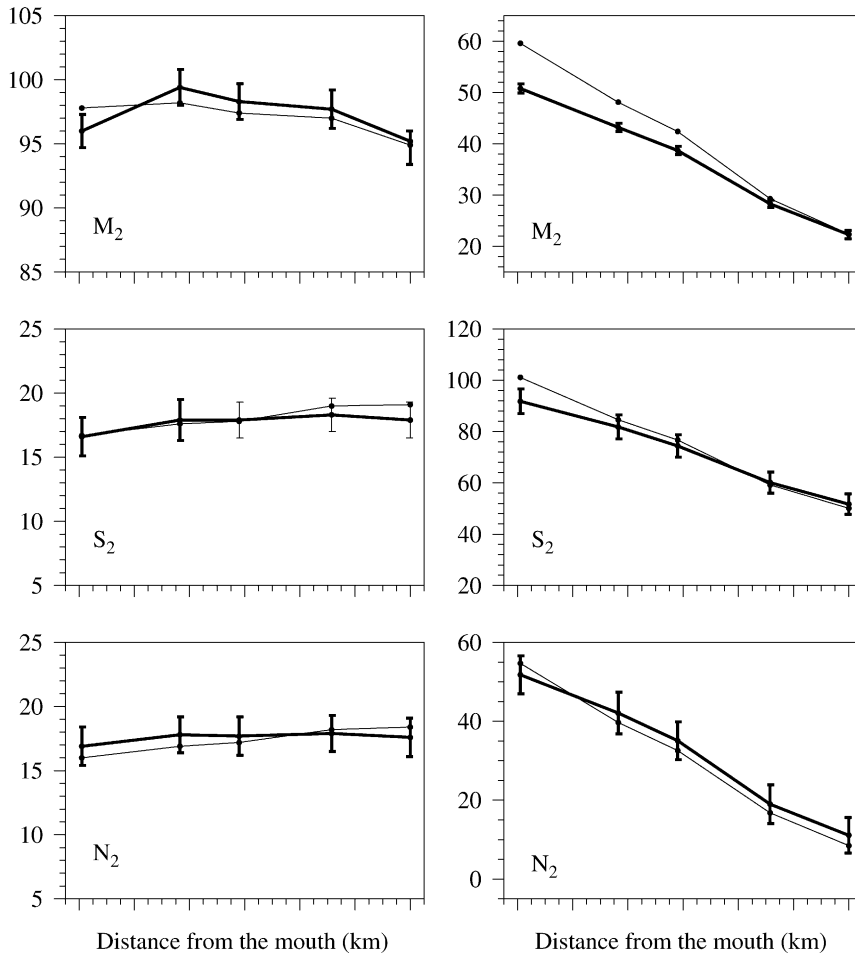


Fig. 5. Comparisons of measured (thick lines) and model-predicted (thin lines) M_2 , S_2 , and N_2 tidal amplitudes (left panel, unit: cm) and phases (right panel, unit: degrees) at along-estuary transects shown in Fig. 1. The error bars were sample standard deviations at a 95% confidence level.

high, which limited phytoplankton production and thus less DO was generated by the photosynthetic process. Meanwhile, inside the estuary, the relatively low salinity (or high nitrification rate from Eq. (4)) and the relatively large ratio of intertidal salt marsh to the estuarine area (or high SOD) resulted in more DO removal from the water column.

The DO concentration was higher in the estuary channel than in the intertidal salt marsh. Since the SOD over the intertidal salt marsh was about twice as much as that in the estuarine channel, when the oxygenated water was transported onto the salt marsh during flood tidal phase, the DO in the water column

over the intertidal salt marsh was quickly consumed and depleted. In addition, our physical model results indicated that the water current in the estuary channel was much larger than in the intertidal salt marsh, resulting in a higher reaeration rate and thus transporting more oxygen from the atmosphere to the water column in the estuarine channel. Fig. 8 also shows that DO concentration in SHW was higher than in SLW inside the estuary. At SHW, the DO concentration was high in the estuary channel and extremely low over the intertidal salt marsh. During ebb tide, the low DO salt marsh water was drained back into the estuarine channel and mixed with relatively high DO water. Af-

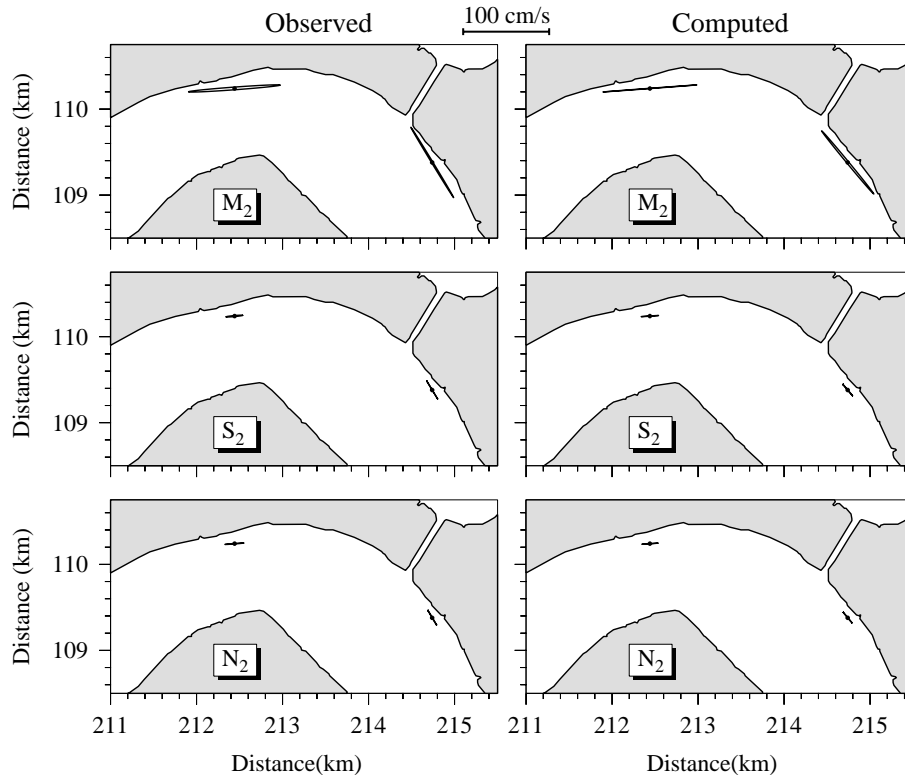


Fig. 6. Comparisons of measured (left panel) and model-predicted (right panel) M_2 , S_2 , and N_2 tidal current ellipses at two current meter-mooring sites ((A) and (E) shown in Fig. 1).

ter complete mixing, the DO concentration in the estuarine water was very low at SLW, especially in the upstream end of the estuary. This implies that the low DO concentration in the Satilla River Estuary during ebb tide and SLW was naturally caused by high SOD over the intertidal salt marsh, not due to anthropogenic activity.

The synoptic distributions of the model-predicted near-surface phytoplankton concentration at SHW and SLW on April 16, 1995 showed the same patterns as DO distributions, i.e., higher concentration in the inner shelf and mouth of the estuary and decreasing concentration when one moves upstream (Fig. 9). Inside the estuary, although observed nutrient concentrations were high enough to support phytoplankton production (Fig. 2), the high turbidity significantly reduced light penetration and limited photosynthesis. Thus, in the Satilla River Estuary, phytoplankton production was mostly limited by light, rather than nutrients. Sim-

ilar light-limited situations have been reported in San Francisco Bay (Alpine and Cloern, 1988) and other estuaries (Cabecadas, 1999).

The phytoplankton concentration at SHW was higher than at SLW, which was possibly related to phytoplankton transport induced by tidal advection. During flood tidal phase, the inward tidal current advected high phytoplankton concentration water from the inner shelf into the estuary. During ebb tidal phase, the outward tidal current advected low phytoplankton concentration estuarine water into the inner shelf. This suggests that tidal forcing played an important role in the chlorophyll-*a* distribution in the Satilla River Estuary.

The synoptic distributions of the model-predicted near-surface ammonium and nitrate concentrations at SHW and SLW on April 16, 1995 showed the same spatial patterns (Figs. 10 and 11). The concentrations were less than $5 \mu\text{g NI}^{-1}$ for ammonium and $10 \mu\text{g}$

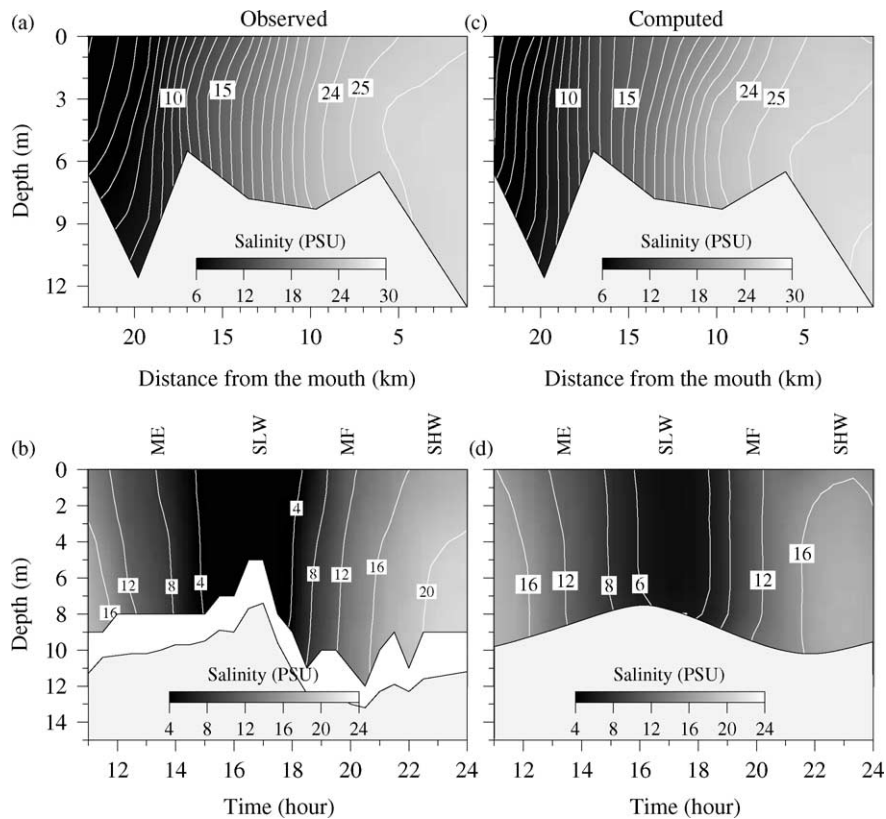


Fig. 7. Comparisons of measured (left panel) and model-predicted (right panel) salinity at an along-estuary transect at SHW and at an anchor site over a tidal cycle on April 16, 1995 in the Satilla River Estuary (ME: maximum ebb; MF: maximum flood; SLW: slack low water; SHW: slack high water). Stations are shown in Fig. 1. Shaded areas in the lower panel include the temporal variation of sea elevation rather than real bottom topography.

NI^{-1} for nitrate in the inner shelf and mouth of the estuary. They increased upstream-ward and reached the maximum values of $30 \mu\text{g NI}^{-1}$ for ammonium and $40 \mu\text{g NI}^{-1}$ for nitrate in the region close to the upstream end. At SHW, the maximum nutrient concentrations were located in the intertidal salt marsh and estuarine channel close to the upstream end. This was related to the phase difference of the tidal current between the two ends of the estuary. The physical model indicates that this phase difference was about 1 h (Zheng et al., 2003a), which means that when the elevation near the mouth of the estuary was at SHW, but it was still in flood tidal phase in the upstream region. Although the bottom stress was not large enough to erode bottom sediment near the mouth of the estuary, it might be larger than the critical stress to cause sediment resuspension and thus nutrient fluxes from

the benthic sediment layer to the water column. The same process occurs at SLW.

The model-predicted nutrient concentrations near the estuary mouth were higher at SLW than at SHW. This was consistent with the model-predicted phytoplankton distribution (Fig. 9). At SHW, phytoplankton concentration near the mouth of the estuary was relatively higher, taking up more nutrients and causing a reduction in nutrient concentrations in this region. Lower phytoplankton concentration at SLW consumed less nutrients and thus nutrient concentrations were relatively high compared to those at SHW.

Model-predicted longitudinal profiles of the water quality components averaged over one M_2 tide cycle in a selected along-estuary transect (shown in Fig. 1) during April 16, 1995 are presented in Fig. 12. The distributions of DO, ammonium nitrogen, nitrate nitro-

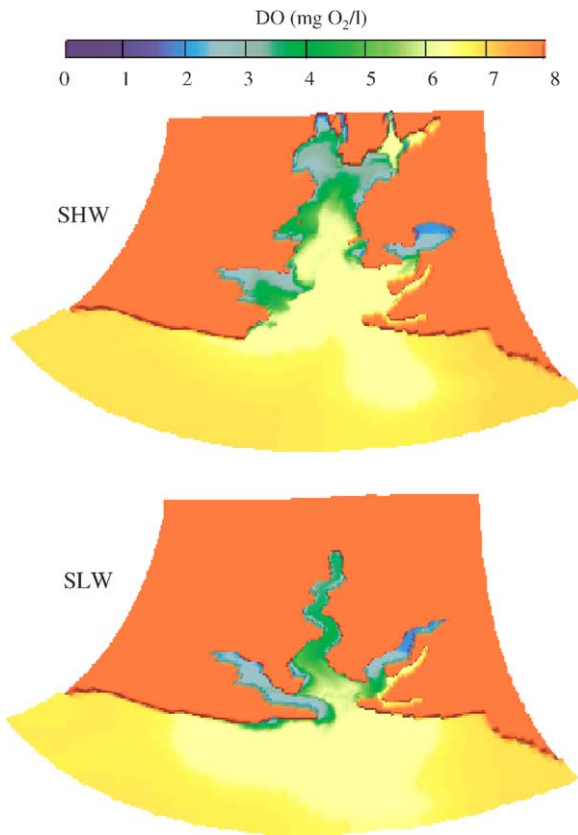


Fig. 8. The synoptic distributions of model-predicted near-surface DO concentration at slack high water (upper) and slack low water (lower) on April 16, 1995.

gen, and ortho-phosphorus were well-mixed vertically and the distributions of chlorophyll-*a*, organic nitrogen, organic phosphorus, and CBOD concentrations had a weak vertical gradient. These vertical gradients were caused by the settling process of these components. The model-predicted concentrations of DO, chlorophyll-*a*, organic nitrogen, organic phosphorus, and CBOD showed a decrease when one moved upstream. Model simulation demonstrated that DO was characterized by extremely low upstream concentrations in the Satilla River Estuary. The DO was higher than $6 \text{ mg O}_2 \text{ l}^{-1}$ at the mouth of the estuary and less than $3 \text{ mg O}_2 \text{ l}^{-1}$ at the upstream end of the estuary. The model-predicted concentrations of the inorganic nutrients (ammonium, nitrate, and ortho-phosphorus) showed low values at both the mouth of the estuary and the upstream end of the estuary and reaching peak

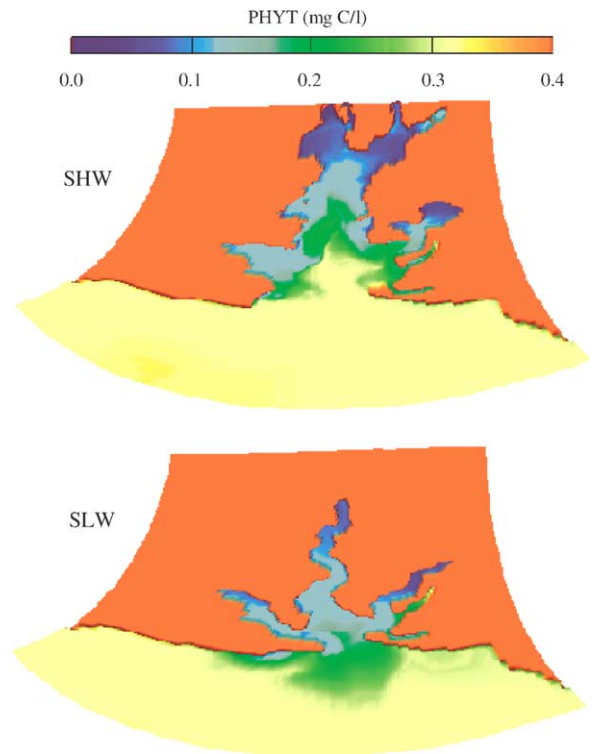


Fig. 9. The synoptic distributions of model-predicted near-surface PHYT concentration at slack high water (upper) and slack low water (lower) on April 16, 1995.

values of $50 \mu\text{g N l}^{-1}$, $130 \mu\text{g N l}^{-1}$, and $17 \mu\text{g P l}^{-1}$, respectively, at approximately 18 km upstream of the estuary. It is interesting to note that the location of maximum inorganic nutrient concentrations was close to the location of maximum suspended sediment concentration (Zheng et al., 2003b).

5.3. Model-data comparison

The model-predicted nutrients (ammonium, nitrate, and ortho-phosphorus) showed good agreement with observational data in the along-estuary transect at SHW on April 16, 1995 during spring tide (Figs. 2 and 13). Around SHW, model-predicted near-surface ammonium nitrogen concentrations reached lowest value of $4 \mu\text{g N l}^{-1}$ near the estuary mouth, increased with distance to approximately $50 \mu\text{g N l}^{-1}$ at 22 km upstream, and then decreased to about $36 \mu\text{g N l}^{-1}$ at 26 km upstream (Fig. 13a), which was consistent with the observed ammonium pattern (Fig. 2a). The am-

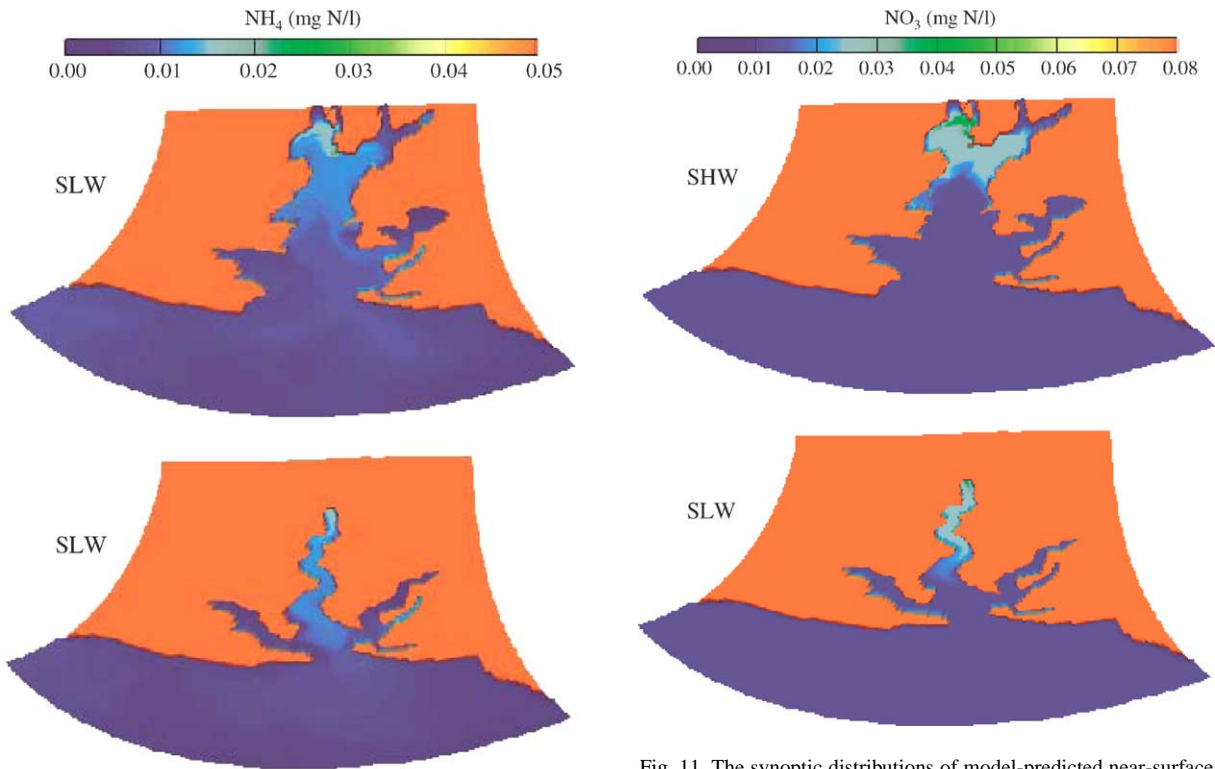


Fig. 10. The synoptic distributions of model-predicted near-surface ammonium concentration at slack high water (upper) and slack low water (lower) on April 16, 1995.

monium concentration was underestimated from 10 to 26 km upstream of the estuary and overestimated from the mouth of the estuary to 10 km upstream. The overall underestimation of the ammonium concentration was $0.2 \mu\text{g N l}^{-1}$. For the nitrate nitrogen, model-predicted values showed that its near-surface concentration was less than $5 \mu\text{g N l}^{-1}$ near the mouth of the estuary, sharply increased to $30 \mu\text{g N l}^{-1}$ 6 km upstream, continuously increased to $70 \mu\text{g N l}^{-1}$ 22 km upstream, and then decreased to $60 \mu\text{g N l}^{-1}$ at the upstream end (Fig. 13b). Again, the nitrate concentration was significantly overestimated in the downstream area and slightly underestimated in the upstream area (Fig. 2b). Overall, the model overestimated the nitrate concentration by $7.9 \mu\text{g N l}^{-1}$. The model-predicted ortho-phosphorus concentration showed a small variation in the along-estuarine section. It was $10 \mu\text{g P l}^{-1}$ near the mouth of the estuary, decreased to a minimum value of $8 \mu\text{g P l}^{-1}$

Fig. 11. The synoptic distributions of model-predicted near-surface nitrate plus nitrite concentration at slack high water (upper) and slack low water (lower) on April 16, 1995.

6 km upstream, and then increased to $13 \mu\text{g P l}^{-1}$ at the upstream end of the estuary (Fig. 13c), which was the same pattern as observations (Fig. 2c). The mean error between observed and model-predicted ortho-phosphorus concentrations was $0.85 \mu\text{g P l}^{-1}$.

Model-predicted near-surface chlorophyll-*a* concentrations in the along-estuarine transect at SHW on April 16, 1995 during the spring tide showed the highest value of $13 \mu\text{g l}^{-1}$ near the mouth of the estuary, decreased to $10 \mu\text{g l}^{-1}$ 6 km upstream, kept a constant value to 16 km upstream, and then decreased to $6 \mu\text{g l}^{-1}$ at the upstream end (Fig. 13d). The model results were in good agreement with observational data in terms of both values and distribution patterns, except near the mouth of the estuary where the model-predicted value was only half of the observed values (Fig. 2d). Overall, the model underestimated the chlorophyll-*a* concentration by about $2.3 \mu\text{g l}^{-1}$.

The coherent picture with underestimation of the chlorophyll-*a* concentration and overestimation of the

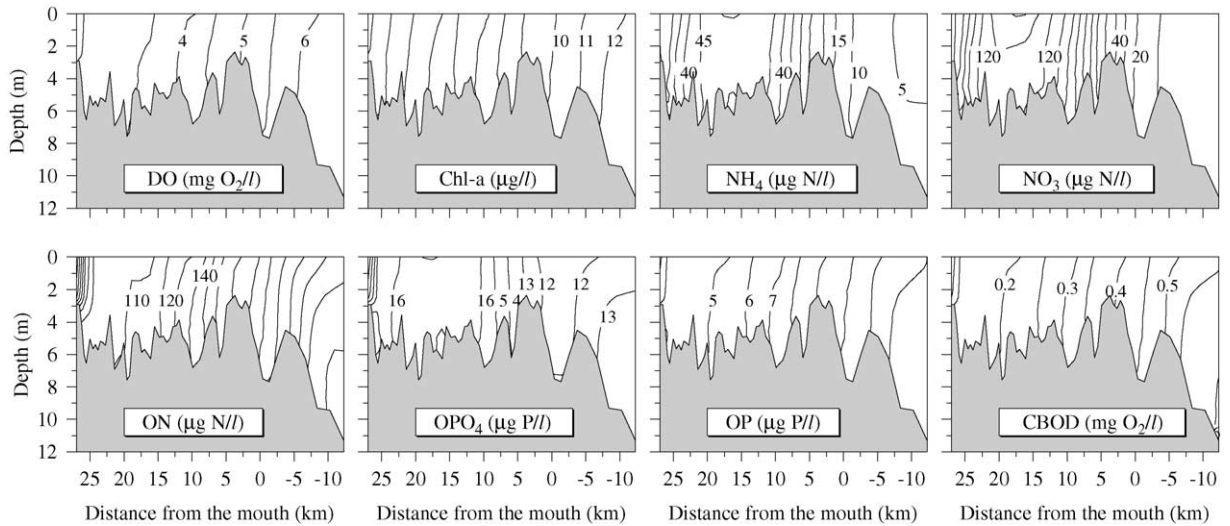


Fig. 12. Model-predicted concentrations of DO, chlorophyll-*a*, ammonium, nitrate, organic nitrogen, ortho-phosphorus, organic phosphorus, and CBOD averaged over one M_2 tidal cycle in the selected along-estuary section (shown in Fig. 1) on April 16, 1995.

nutrient concentration near the mouth of the estuary suggested that a large uptake rate of nutrients should be specified in the model, even though the overestimation of the nutrient concentration also might be due to an overestimation of nutrient flux from the bottom sediment layer. Three mechanisms can lead to underestimation of the ammonium concentration in the upstream region of the estuary. First, the model may have underestimated the ammonium fluxes from the bottom sediment layer. Second, the ammonium loaded from the intertidal salt marsh, which is excluded in our model, might make an important contribution in maintaining the ammonium level in the estuary. Third, the model may have overestimated the nitrification rate. Similarly, the first two mechanisms might be responsible for underestimation of nitrate concentration in the upstream region. The fact that the nutrient flux was overestimated near the mouth of the estuary and underestimated in the upstream region suggests that the coefficients in Eq. (5) might be spatially dependent.

5.4. Sensitivity analysis

In the following sensitivity analysis experimental runs, the initial concentrations of water quality compo-

nents and parameters used in the water quality model are the same as those used in the standard experimental run, except as specially noted in different experiment cases. The model-predicted results will be compared with those predicted from the standard experimental run to examine the impact of physical and biogeochemical processes on distributions of water quality components.

When the flooding/drying process over the intertidal salt marsh was removed from the model (called experimental run I), the DO concentration showed a small variation in the estuary, ranging from $7.0 \text{ mg O}_2 \text{ l}^{-1}$ near the estuary mouth to $6.0 \text{ mg O}_2 \text{ l}^{-1}$ at the upstream end (Fig. 14). CBOD concentration had a value of $0.5 \text{ mg O}_2 \text{ l}^{-1}$ near the estuary mouth and gradually decreased to $0.4 \text{ mg O}_2 \text{ l}^{-1}$ at the upstream end. The concentrations of chlorophyll-*a*, organic nitrogen, and organic phosphorus exhibited the same pattern as that of CBOD, i.e., highest near the estuary mouth and decreasing upstream. Their values range from 13 µg l^{-1} , 250 µg N l^{-1} , and 12 µg P l^{-1} to 10 µg l^{-1} , 200 µg N l^{-1} , and 9 µg P l^{-1} , respectively. The concentrations of ammonium and nitrate nitrogen were extremely low with values less than 5 µg N l^{-1} across the entire transect. The ortho-phosphorus concentration showed a high value of about 13 µg P l^{-1} in the region from 0

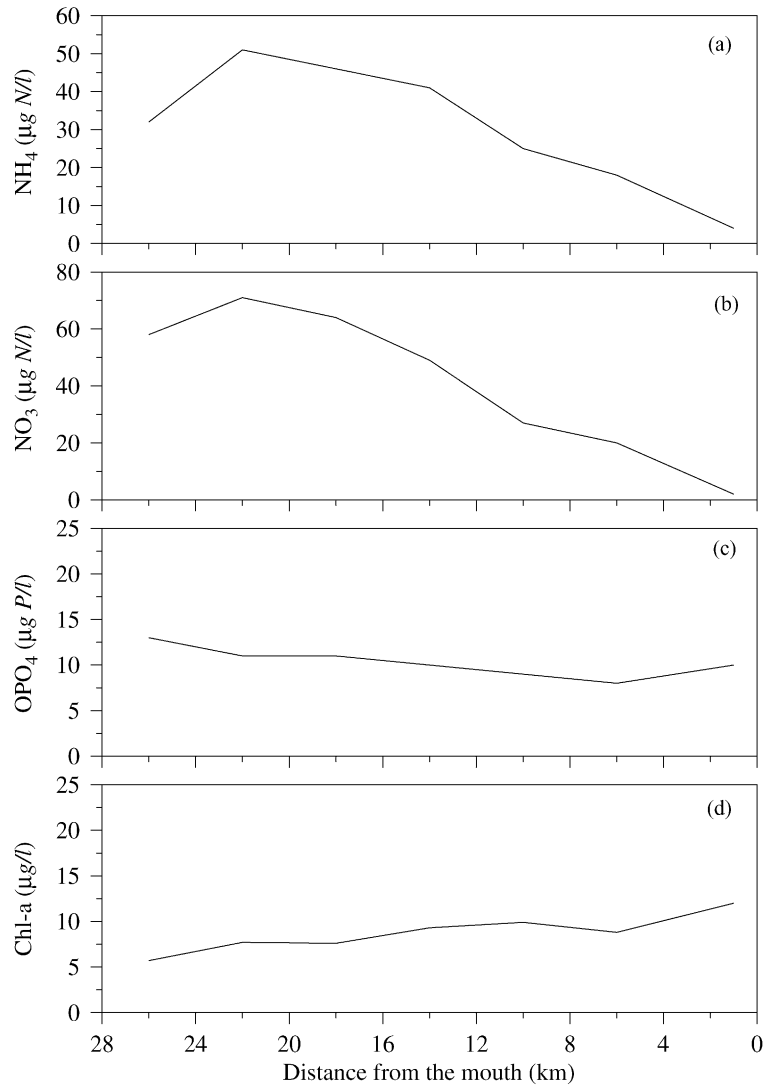


Fig. 13. Model-predicted concentrations of ammonium (a), nitrate plus nitrite (b), ortho-phosphorus (c), and chlorophyll-*a* (d) in an along-estuary transect at slack high water on April 16, 1995.

to 10 km upstream from the estuary mouth, sharply decreased to $4 \mu\text{g P l}^{-1}$ at 20 km upstream, and then gradually decreased to approximately $3 \mu\text{g P l}^{-1}$ at the upstream end of the estuary.

Compared with results from the standard run, the section-averaged concentrations of DO, CBOD, chlorophyll-*a*, organic nitrogen, and organic phosphorus were about $3 \text{ mg O}_2 \text{ l}^{-1}$, $0.2 \text{ mg O}_2 \text{ l}^{-1}$, $2.5 \mu\text{g l}^{-1}$, $100 \mu\text{g N l}^{-1}$, and $5 \mu\text{g P l}^{-1}$ higher, respectively,

while the section-averaged concentrations of ammonium, nitrate, and ortho-phosphorus were about $29 \mu\text{g N l}^{-1}$, $42 \mu\text{g N l}^{-1}$, and $0.5 \mu\text{g P l}^{-1}$ lower, respectively (Fig. 14). The DO in the Satilla River Estuary was mainly controlled by the processes associated with reaeration, photosynthesis, SOD, nitrification, and oxidation of CBOD. When the intertidal salt marsh was removed, the hydrodynamic model indicates that model-predicted tidal current would be

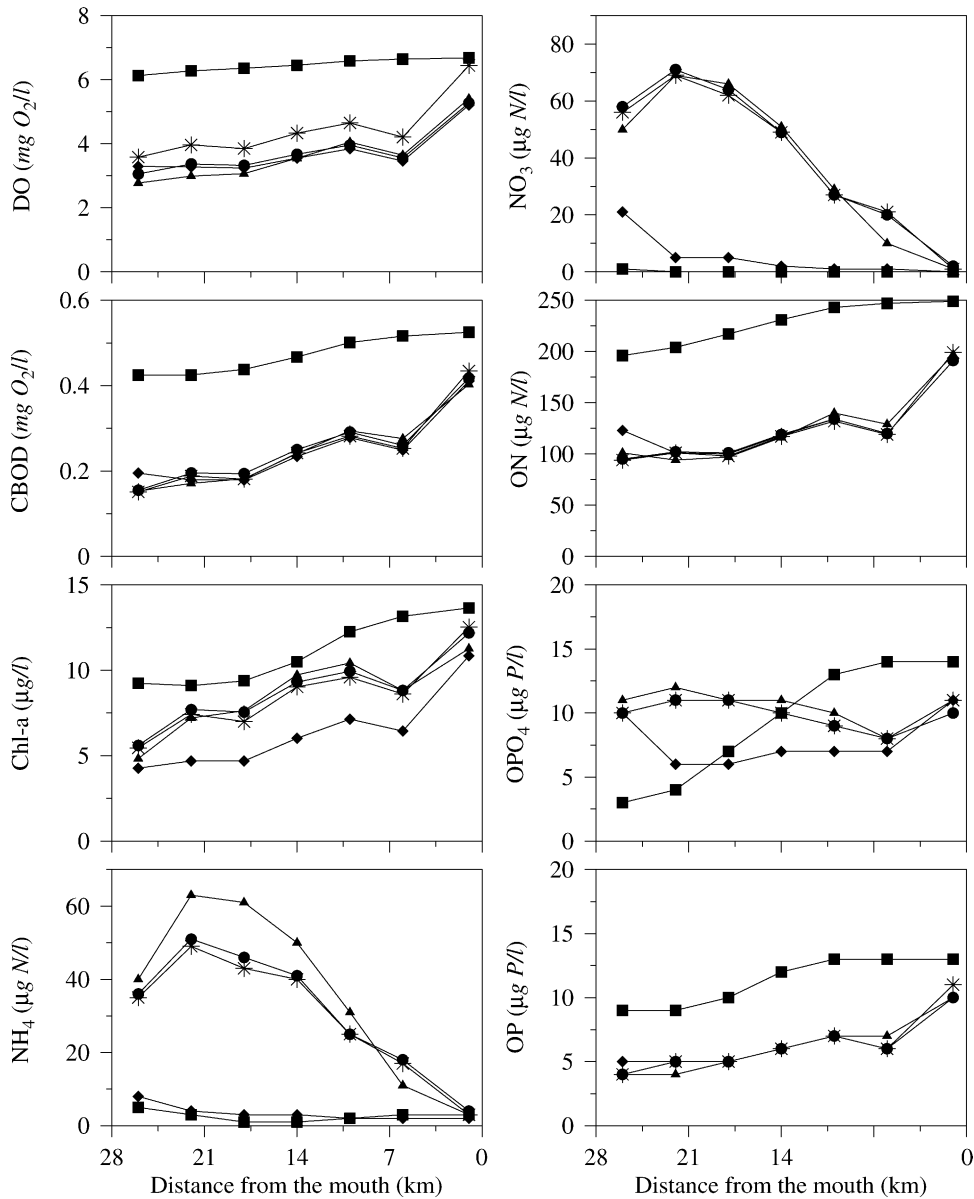


Fig. 14. Model-predicted concentrations of DO, CBOD, chlorophyll-*a*, ammonium, nitrate, organic nitrogen, ortho-phosphorus, and organic phosphorus in an along-estuary transect at SHW on April 16, 1995 for different model conditions. Filled circles were the standard run, in which the model included tidal forcing, real-time river discharge, flooding/drying over the intertidal salt marsh, and nutrient fluxes from the bottom sediment layer. Filled squares were referred to as experimental run I, which had the same model setup as the standard run except the flooding/drying process over the intertidal salt marsh was excluded. Filled diamonds were referred to as experimental run II, which had the same model setup as the standard run except nutrient fluxes from the bottom sediment layer were excluded. Filled triangles were referred to as experimental run III, which had the same model setup as the standard run except the salinity was specified as constant at 35 PSU. Stars were referred to as experimental run IV, which had the same model setup as the standard run except heterotrophic bacterial respirations were excluded.

underestimated by 50% of its amplitude. The small tidal current would result in a small reaeration rate, causing a reduction in the oxygen exchange between the atmosphere and the water column. Also, the oxidation of CBOD consumed more DO in the water column. Thus, if DO was dominantly affected by reaeration and oxidation of CBOD, the DO concentration would decrease, rather than increase in the Satilla River Estuary when the flooding/drying process over the intertidal salt marsh was removed. This implies that some other processes were responsible for the increase of DO concentration. Firstly, as ammonium nitrogen concentration decreased when intertidal salt marsh was excluded, the less DO was consumed due to nitrification. Secondly, the relatively high phytoplankton concentration produced more DO. Thirdly, since the intertidal salt marsh was removed from the model, the large loss of DO caused by high SOD rate over the intertidal salt marsh was ignored, which could significantly promote the DO concentration. Our model experimental run showed that the first two processes can increase DO concentration of about $0.4 \text{ mg O}_2 \text{ l}^{-1}$, which accounted for 15% of the total DO increase observed in this experimental run, and the third process suggested that high SOD rate over the intertidal salt marsh was the most important process in controlling DO balance. This result implies that low DO concentration found from observation in this estuary (Pomeroy et al., 2000) was mainly caused by a high SOD over the intertidal salt marsh, rather than by processes associated with anthropogenic activities. Our model results were consistent with modelling findings using one-dimensional water quality model (DYRESM) conducted by Schladow and Hamilton (1997), which indicated that in lakes and reservoirs the SOD was the most important factors to effect DO in the water column.

Previous observations and modelling studies suggest that water current over the intertidal salt marsh was relatively weak (Zheng et al., 2003a). The particulate organic matter, CBOD, and phytoplankton can easily settle to the bottom when they were advected onto the intertidal marsh during the flood tidal phase. Because our model did not include resuspension of particulate materials deposited in the bottom sediment layer, the intertidal salt marsh acted as a sink for these materials. Thus, excluding intertidal salt

marsh in the model would increase the concentrations of these particulate materials. Model-predicted concentrations of CBOD, organic nitrogen, and organic phosphorus in this model experimental run were about twice as much as those predicted in standard run, suggesting that flooding/drying over the intertidal salt marsh was an important process for controlling these water quality components in the Satilla River Estuary.

Removing flooding/drying processes over the intertidal salt marsh, model-predicted concentrations of ammonium and nitrate were significantly reduced, but the concentration of ortho-phosphorus varied slightly. Two mechanisms were possibly responsible for the low concentrations of ammonium and nitrate. Firstly, the model-predicted phytoplankton concentration was relatively high in this experimental run. There will be more nutrient consumed by phytoplankton uptake. Secondly, as stated above, the model-predicted bottom stress was significantly reduced when flooding/drying processes over the intertidal salt marsh were removed. From Eq. (5), the nutrient fluxes from the bottom sediment layer would be considerably decreased. It is interesting to note that the ortho-phosphorus concentration increased from 0 to 15 km upstream and then decreased in the rest of the region in this experimental run. The upstream decrease might be caused by less flux from bottom sediment layer, while increase in the downstream might be related to the fact that a relatively large amount was recycled from dead phytoplankton converted from organic phosphorus by bacterial decomposition.

In the experimental run II, nutrient fluxes from the bottom sediment layer were eliminated. Model-predicted near-surface concentrations of eight water quality components in the along-estuary transect at SHW on April 16, 1995 were given in Fig. 14. The ammonium concentration was less than $10 \mu\text{g N l}^{-1}$ in the entire transect. The nitrate concentrations were extremely low near the estuary mouth, gradually increased to $5 \mu\text{g N l}^{-1}$ at 22 km upstream, and then sharply increased to about $20 \mu\text{g N l}^{-1}$ at the upstream end of the estuary. The ortho-phosphorus concentration showed a high value of $10 \mu\text{g P l}^{-1}$ at both estuary mouth and upstream end and a low value of $5 \mu\text{g P l}^{-1}$ in the mid-section. Compared with the standard run, the concentrations of DO, CBOD, organic nitrogen, and organic phosphorus were not significantly

changed, but the concentrations of chlorophyll-*a*, ammonium, nitrate, and ortho-phosphorus became lower. The relatively low phytoplankton concentration in this case was mainly caused by low nutrient levels. The sharp increase in nitrate concentration at the upstream end was the result of high nitrification, rather than physical processes.

In the modelling studies of depth-averaged WASP (Tufford and McKellar, 1999) and three-dimensional CE-QUAL-ICM (Cercio, 2000), they found that nutrient releases from sediment are significantly contributing to ammonium and nitrate concentrations in the estuary. These results were confirmed by our study in the Satilla River Estuary. According to experimental runs I and II, the results suggest that nutrient (ammonium and nitrate) fluxes from the bottom sediment layer were an important nutrient sources and played a critical role in maintaining these nutrient levels, but did not significantly affect DO, CBOD, organic nitrogen, and organic phosphorus concentrations in the Satilla River Estuary. The mechanisms responsible for ortho-phosphorus changed in different sections of the estuary. From 0 to 10 km upstream, the ortho-phosphorus concentration was dominantly controlled by mineralization of organic phosphorus and recycling from dead phytoplankton. From 10 to 22 km, it was controlled by both phytoplankton uptake and flux from the bottom sediment layer. From 22 km to the upstream end, it was mainly controlled by phytoplankton uptake.

When salinity was fixed at 35 PSU in the entire computational spatial and temporal domain (called experimental run III), model-predicted distribution patterns of the eight water quality components in the along-estuary transect at SHW on April 16, 1995 were the same as those predicted in the standard run (Fig. 14). Compared with results predicted by the standard run, the concentrations of all water quality components except ammonium were only slightly different. Model-predicted ammonium concentration was about 10–20 $\mu\text{g N l}^{-1}$ higher in the mid-section where the salinity was in the range of 5–15 PSU (Zheng et al., 2003a). In addition, model-predicted nitrate concentration at the upstream end of the estuary was about 10 $\mu\text{g N l}^{-1}$ lower. When salinity was specified as constant, the physical model became barotropic. Due to elimination of buoyancy-driven currents that cancel the inward

current during flood tide, the model-predicted bottom stress was large in this model run and resulted in large nutrient fluxes from the bottom sediment layer. Thus, the ammonium concentration significantly increased and ortho-phosphorus concentration also slightly increased. It should be noted that the nitrate concentration decreased in the upstream end, rather than increasing like ammonium concentration. This implies that other important physical or internal biogeochemical processes were controlling its distribution. From Eq. (4), the nitrification rate decreased when salinity level increased. Thus, 35 PSU salinity in the model would reduce the amount of conversion from ammonium to nitrate, leading to relatively high ammonium and low nitrate concentrations. The result suggests that nitrification was an important process in controlling nitrogen levels in the Satilla River Estuary.

When the heterotrophic bacterial respiration process was excluded, except DO, model-predicted concentrations of the water quality components in the along-estuary transect at SHW on April 16, 1995 were the same as those predicted in the standard run (Fig. 14). This implies that in the water quality model developed for the Satilla River Estuary, the heterotrophic bacterial respiration affected only on the DO concentration. The model results indicate that without the inclusion of this process, DO concentration can increase about 0.5 mg $\text{O}_2 \text{l}^{-1}$ along the entire estuarine transect, which accounted for 15% of total DO concentration in the upstream region of this estuary. This suggests that the heterotrophic respiration should be included in the water quality model study in the Satilla River Estuary.

6. Conclusions

A coupled water quality and physical model was used to examine the impact of physical, chemical, and biogeochemical processes and their interaction on spatial distribution of water quality components in the Satilla River Estuary, Georgia. The physical model was driven by M_2 , S_2 , and N_2 tidal forcings at the open boundary in the inner shelf of SAB and real-time river discharge at the upstream end of the estuary, with inclusion of the flooding/draining cycle of the intertidal

salt marshes. The initial salinity condition was specified based on observations taken along the estuary. The water quality model was a modified WASP5 model with inclusion of processes of photosynthesis, reaeration, nitrification, denitrification, oxidation of CBOD, mineralization, SOD, nutrient uptake by phytoplankton, recycling from dead phytoplankton, and nutrient fluxes from the bottom sediment layer.

Given initial spatially horizontally and vertically uniform distributions of water quality components, model-predicted concentrations of inorganic nutrients (ammonium, nitrate plus nitrite, and ortho-phosphorus) and chlorophyll-*a* in an along-estuary transect were in good agreement with observations data taken at slack high water on April 16, 1995 during spring tide. Model studies suggest that water quality in this estuary was impacted by physical, chemical, and biogeochemical processes and their interactions. DO balance was dominantly controlled by the SOD process. Low DO concentration in the Satilla River Estuary was due to the high SOD over the intertidal salt marsh and a large ratio of salt marsh area to estuary channel area, which was a naturally occurring condition, rather than anthropogenic activities. Model experiments showed that nutrient fluxes from the bottom sediment layer were the most important nutrient sources and played a critical role in maintaining nutrient levels in this estuary. Ignoring these processes would lead to more than 90% of underestimation for ammonium and nitrate concentrations. Nitrification was another important process in controlling nutrient distribution, especially in the region with high turbidity and low salinity water. The intertidal salt marsh acted as a main sink for particulate materials and must be included in water quality modelling studies.

Acknowledgements

This research was supported by the Georgia Sea Grant College Program under grant numbers NA26RG0373 and NA66RG0282. We want to thank Drs. S. Joye, M. Alber, R. Ambrose, L. Pomeroy, W. Wiebe, and R. Walker for their helpful discussion during the model development. We would like to thank Drs. J. Blanton, W. Wiebe, M. Alber, and L. Pomeroy for permission to use their GALMER observational data. Alice Chamber provided us digitized

2-m elevation data set and her contribution should be credited. We thank Dr. Mac Rawson, Director of the Georgia Sea Grant College Program, for his encouragement and help in the project organization. We also want to thank J. Sheldon for providing us the information about nutrient measurement methods. Two anonymous reviewers have provided many critical constructive suggestions, which really helped us improve the final version of this manuscript.

Appendix A

The mathematical expression for the internal sources or sinks (S_i , $i = 1, 8$) of the water quality variables shown in Eq. (2) are given as follows. C_i ($i = 1, 8$) were corresponding to the concentrations of dissolved oxygen, phytoplankton, carbonaceous chemical oxygen demand, ammonium nitrogen, nitrate and nitrite nitrogen, ortho-phosphorus, organic nitrogen, and organic phosphorus, respectively.

A.1. Dissolved oxygen (DO)

$$S_1 = k_{r1}\theta_{r1}^{(T-20)}(C_s - C_1) - k_{d1}\theta_{r1}^{(T-20)}\frac{C_1C_3}{K_{BOD} + C_1} - \frac{32}{12}k_{r2}\theta_{r1}^{(T-20)}C_2 - \frac{32}{14}2k_{ni}\theta_{ni}^{(T-20)}\frac{C_1C_4}{K_{NITR} + C_1} + G_P\left[\frac{32}{12} + \frac{48}{14}a_{nc}(1 - P_{NH_4})\right]C_2 - \frac{SOD}{D}\theta_{SOD}^{(T-20)} - k_{r3} \quad (A.1)$$

A.2. Phytoplankton (PHYT)

$$S_2 = G_P C_2 - D_P C_2 - \frac{w_{2S}}{D} C_2 \quad (A.2)$$

A.3. Carbonaceous biochemical oxygen demand (CBOD)

$$S_3 = a_{oc}(k_{par} + k_{grz})C_2 - k_{d1}\theta_{d1}^{(T-20)}\frac{C_1C_3}{K_{BOD} + C_1} - \frac{w_{3S}(1 - f_{D3})}{D}C_3 - \frac{5}{4} \times \frac{32}{12} \times \frac{12}{14}k_{dn}\theta_{dn}^{(T-20)}\frac{C_5K_{NO_3}}{K_{NO_3} + C_1} \quad (A.3)$$

A.4. Ammonium nitrogen (NH_4)

$$S_4 = a_{nc} D_P (1 - f_{on}) C_2 + k_{m1} \theta_{m1}^{(T-20)} \frac{C_2 C_7}{K_{mPc} + C_2} - a_{nc} G_P P_{NH_4} C_2 - k_{ni} \theta_{ni}^{(T-20)} \frac{C_1 C_4}{K_{NITR} + C_1} + B_1 \quad (A.4)$$

A.5. Nitrate and nitrite nitrogen (NO_3)

$$S_5 = k_{ni} \theta_{ni}^{(T-20)} \frac{C_1 C_4}{K_{NITR} + C_1} - a_{nc} G_P (1 - P_{NH_4}) C_2 - k_{dn} \theta_{dn}^{(T-20)} \frac{C_5 K_{NO_3}}{K_{NO_3} + C_1} + B_2 \quad (A.5)$$

A.6. Ortho-phosphorus (OPO_4)

$$S_6 = a_{pc} D_P (1 - f_{op}) C_2 + k_{m2} \theta_{m2}^{(T-20)} \frac{C_2 C_8}{K_{mPc} + C_2} - a_{pc} G_P C_2 + B_3 \quad (A.6)$$

A.7. Organic nitrogen (ON)

$$S_7 = a_{nc} D_P f_{on} C_2 - k_{m1} \theta_{m1}^{(T-20)} \frac{C_2 C_7}{K_{mPc} + C_2} - \frac{w_{7S}(1 - f_{D7})}{D} C_7 \quad (A.7)$$

A.8. Organic phosphorus (OP)

$$S_8 = a_{pc} D_P f_{op} C_2 - k_{m2} \theta_{m2}^{(T-20)} \frac{C_2 C_8}{K_{mPc} + C_2} - \frac{w_{8S}(1 - f_{D8})}{D} C_8 \quad (A.8)$$

where the definition for each parameters used in the above equations is given in Table 2.

The aeration rate k_{r1} is chosen as the maximum value of flood-induced reaeration (Covar, 1976) and wind-induced reaeration (O'Connor, 1983). Dissolved oxygen saturation concentration, C_s , is determined as a function of salinity (S) and temperature (T) via the following equation (APHA, 1985):

$$\ln C_s = -139.34 + (1.5757 \times 10^5) T^{-1} - (6.6423 \times 10^7) T^{-2} + (1.2438 \times 10^{10}) T^{-3} - (8.6219 \times 10^{11}) T^{-4} - 0.5535 \times S(0.031929 - 19.428 T^{-1} + 3867.3 T^{-2}) \quad (A.9)$$

The growth rate of phytoplankton G_P is determined by the ambient temperature, incident irradiance intensity, and nutrient availability. It can be expressed as:

$$G_P = k_{gr} \theta_{gr}^{(T-20)} f_1(N) f_2(I) \quad (A.10)$$

where $f_1(N)$ is the nutrient limitation factor that is assumed to follow the Michaelis–Menten function, i.e., $f_1(N) = \min((C_4 + C_5)/(K_{mN} + C_4 + C_5), (C_6/K_{mP} + C_6))$ and $f_2(I)$ is the light limitation factor.

The reduction rate of phytoplankton included its endogenous respiration, death rate due to the effect of viral lysis, and grazing by zooplankton. The death rate of phytoplankton was expressed as:

$$D_P = (k_{r2} + k_{par} + k_{grz}) \theta_{gr}^{(T-20)} \quad (A.11)$$

During phytoplankton growth, both NH_4 and NO_3 were available for uptake. For physiological reasons, the preferred form for phytoplankton uptake was NH_4 . The ammonium preference form was given as:

$$P_{NH_4} = \frac{C_4 C_5}{(K_{mN} + C_4)(K_{mN} + C_5)} + \frac{C_4 K_{mN}}{(C_4 + C_5)(K_{mN} + C_5)} \quad (A.12)$$

References

- Alpine, A.E., Cloern, J.E., 1988. Phytoplankton growth-rates in a light-limited environment, San Francisco Bay. *Mar. Ecol. Progr. Ser.* 44, 167–173.
- Ambrose Jr., R.B., Wool, T.A., Martin, J.L., 1993. The Water Quality Analysis Simulation Program, WASP5, Part A: Model Documentation. U.S. Environmental Protection Agency, Athens, Georgia, 202 pp.
- APHA (American Public Health Association), 1985. Standard Methods for the Examination of Water and Wastewater, 15th ed. APHA, Washington, DC.
- Beck, K.C., Reuter, J.H., Perdue, E.M., 1974. Organic and inorganic geochemistry of some coastal plain rivers of southeastern United States. *Geochim. Cosmochim. Acta* 38, 341–364.
- Blake, A.C., Kineke, G.C., Milligan, T.G., Alexander, C.R., 2001. Sediment trapping and transport in the ACE basin, South Carolina. *Estuaries* 24, 721–733.
- Blanton, J.O., 1996. Reinforcement of gravitational circulation by wind. In: Aubrey, D.G., Friedrichs, C.T. (Eds.), *Buoyancy Effects on Coastal and Estuarine Dynamics*. Coastal Estuarine Studies, American Geophysical Union, Washington, DC, pp. 47–58.

- Blanton, J.O., Alexander, C.R., Alber, M., Kineke, G., 1999. The mobilization and deposition of mud deposits in a coastal plain estuary. *Limnologia* 29, 293–300.
- Blumberg, A.F., 1993. A Primer of ECOM_{si}. Technical Report. HydroQual, Inc., Mahwah, New Jersey.
- Bricker, S., Clement, C., Pirhall, D., Orlando, S., Farrlow, D., 1999. National Estuarine Eutrophication Assessment: A Summary of Conditions, Historical Trends, and Future Outlook. National Oceanic and Atmospheric Administration, Silver Spring, Maryland.
- Cabecadas, L., 1999. Phytoplankton production in the Tagus estuary (Portugal). *Oceanol. Acta* 22, 205–214.
- Casulli, V., 1990. Semi-implicit finite-difference methods for the two-dimensional shallow water equations. *J. Comput. Phys.* 86, 56–74.
- Cerco, C.F., 2000. Chesapeake Bay eutrophication model. In: Hobbie, J.E. (Ed.), *Synthetic Approach to Research and Practice. Estuarine Science*, Washington, DC, pp. 363–404.
- Chen, C., 2003. *Marine Ecosystem Dynamics and Modeling*. New Frontier of Sciences. Higher Education Press of China, 404 pp.
- Chen, C., Beardsley, R., 1998. Tidal mixing and cross-frontal particle exchange over a finite amplitude asymmetric bank: a model study with application to Georges Bank. *J. Mar. Res.* 56, 1163–1201.
- Chen, C., Beardsley, R., 2002. Cross-frontal water exchange on Georges Bank: modeling exploration of the US GLOBEC/Georges Bank phase III study. *J. Oceanogr.* 58, 403–420.
- Costanza, R., d'Arge, R., deGroot, R., Farber, S., Grasso, M., Hannon, B., Limburg, K., Naeem, S., Oneil, R.V., Paruelo, J., Raskin, R., Sutton, P., vandenBelt, M., 1997. The value of the world's ecosystem services and natural capital. *Nature* 387, 253–260.
- Covar, A.P., 1976. Selecting the proper reaeration coefficient for use in water quality models. Presented at the U.S. EPA conference on Environmental Simulation Modeling, 19–22 April 1976, Cincinnati, Ohio.
- Cowan, J.L.W., Boynton, W.R., 1996. Sediment-water oxygen and nutrient exchanges along the longitudinal axis of Chesapeake Bay: seasonal patterns, controlling factors and ecological significance. *Estuaries* 19, 562–580.
- Cowan, J.L.W., Pennock, J.R., Boynton, W.R., 1996. Seasonal and interannual patterns of sediment-water nutrient and oxygen fluxes in Mobile Bay, Alabama (USA): regulating factors and ecological significance. *Mar. Ecol. Progr. Ser.* 141, 229–245.
- Dame, R.M., Alber, M., Allen, D., Mallin, M., Montague, C., Lewitus, A., Chalmers, A., Gardner, R., Gilman, C., Kjerfve, B., Pinckney, J., Smith, N., 2000. Estuaries of the South Atlantic Coast of North America: their geographical signatures. *Estuaries* 23, 793–819.
- D'Elia, C.F., Kaumeyer, N.L., Keefe, C.L., Shaw, D.L., Wood, K.V., Zimmermann, C.F., 1987. Standard Operating Procedures. Nutrient Analytical Services Laboratory, Chesapeake Biological Laboratory, Solomons, Maryland.
- Di Toro, D.M., O'Connor, D.J., Thomann, R.V., 1971. A dynamic model of the phytoplankton population in the Sacramento-San Joaquin Delta. *Adv. Chem. Ser.* 106, 131–180.
- Galperin, B., Kantha, L.H., Hassid, S., Rosati, A., 1988. A quasi-equilibrium turbulent energy model for geophysical flows. *J. Atmos. Sci.* 45, 55–62.
- Giblin, A.G., Hopkinson, C.S., Tucker, J., 1997. Benthic metabolism and nutrient cycling in Boston Harbor, Massachusetts. *Estuaries* 20, 346–364.
- Howarth, R., Swaney, D., Butler, T., Marino, R., 2000. Climatic control on eutrophication of the Hudson River estuary. *Ecosystems* 3, 210–215.
- James, R.T., Bierman Jr., V.J., 1995. A preliminary modeling analysis of water quality in Lake Okeechobee, Florida: calibration results. *Water Res.* 12, 2755–2766.
- James, R.T., Martin, J., Wool, T., Wang, P.F., 1997. A sediment resuspension and water quality mode of Lake Okeechobee. *J. Am. Water Resour. Assoc.* 33, 661–680.
- Jones, M.N., 1984. Nitrate reduction by shaking with cadmium: alternative to cadmium columns. *Water Res.* 18, 643–646.
- Kemp, W.M., Smith, E.M., MarvinDipasquale, M., Boynton, W.R., 1997. Organic carbon balance and net ecosystem metabolism in Chesapeake Bay. *Mar. Ecol. Progr. Ser.* 150, 229–248.
- Koroleff, F., 1983. Determination of ammonia. In: Grasshoff, K., Ehrhardt, M., Kremling, K. (Eds.), *Methods of seawater analysis*, 2nd ed. (revised and extended). Verlag Chemie, Weinheim, pp. 150–157.
- Mellor, G.L., Yamada, T., 1982. Development of a turbulence closure model for geophysical fluid problems. *Rev. Geophys.* 20, 851–875.
- Monod, J., 1949. The growth of bacterial cultures. *Annu. Rev. Microbiol.* 3, 371–394.
- O'Connor, D.J., 1983. Wind effects on gas-liquid transfer coefficients. *J. Environ. Eng.* 109, 731–752.
- Paerl, H.W., 1988. Nuisance phytoplankton blooms in coastal estuarine and inland waters. *Limnol. Oceanogr.* 33, 823–847.
- Pakulski, J.D., Benner, R., Whiteledge, T., Amon, R., Eadie, B., Cifuentes, L., Ammerman, J., Stockwell, D., 2000. Microbial metabolism and nutrient cycling in the Mississippi and Atchafalaya River plumes. *Estuaries* 50, 173–184.
- Pomeroy, L.R., Blanton, J.O., Paffenhöfer, G.A., Damn, K.L.V., Verity, P.G., Windom, H.L., Lee, T.N., 1993. Inner shelf processes. In: Menzel, D.W. (Ed.), *Ocean Processes: U.S. Southeast Continental Shelf*, pp. 9–43.
- Pomeroy, L.R., Sheldon, J.E., Sheldon, W.M., Blanton, J.O., Amft, J., Peters, F., 2000. Seasonal changes in microbial processes in estuarine and continental shelf waters of the southeastern U.S.A. *Estuarine, Coastal Shelf Sci.* 51, 415–428.
- Pomeroy, L.R., Shenton, L.R., Jones, R.D.H., Reimold, R.J., 1972. Nutrient flux in estuaries. In: Likens, G.E. (Ed.), *Nutrients and Eutrophication: The Limiting-nutrient Controversy*. American Society of Limnology and Oceanography, Special Symposium 1. Lawrence, Kansas, pp. 274–291.
- Pomeroy, L.R., Wiegert, R.G., 1981. *The Ecology of a Salt Marsh*. Springer-Verlag, New York, 271 pp.
- Schladow, S.G., Hamilton, D.P., 1997. Prediction of water quality in lakes and reservoirs: modeling calibration, sensitivity analysis, and application. *Ecol. Model.* 96, 111–123.
- Shen, J., 1996. *Water Quality Modeling as an Inverse Problem*. Ph.D. Dissertation. The College of William and Mary in Virginia, 140 pp.

- Smolarkiewicz, P.K., 1984. A fully multidimensional positive definite advection transport algorithm with small implicit diffusion. *J. Comput. Phys.* 54, 325–362.
- Tufford, D.L., McKellar, H.N., 1999. Spatial and temporal hydrodynamic and water quality modeling analysis of a large reservoir on the South Carolina (USA) coastal plain. *Ecol. Model.* 114, 137–173.
- Verity, P.G., Yoder, J.A., Bishop, S.S., Nelson, J.R., Craven, D.B., Blanton, J.O., Robertson, C.Y., Tronzo, C.R., 1993. Composition, productivity and nutrient chemistry of a coastal ocean planktonic food web. *Continental Shelf Res.* 13, 741–776.
- Vörösmarty, C.J., Loder, T.C., 1994. Spring-neap tidal contrasts and nutrient dynamics in a marsh-dominated estuary. *Estuaries* 17, 537–551.
- Wang, P.F., Martin, J., Morrison, G., 1999. Water quality and eutrophication in Tampa Bay Florida. *Estuarine, Coastal Shelf Sci.* 49, 1–20.
- Weber, A.H., Blanton, J.O., 1980. Monthly mean wind fields for the South Atlantic Bight. *J. Phys. Oceanogr.* 10, 1256–1263.
- Windom, H.L., Dunstan, W.M., Gardner, W.S., 1975. River input of inorganic phosphorus and nitrogen to the southeastern salt-marsh estuarine environment. In: Howell, F.G., Gentry, J.B., Smith, M.H. (Eds.), *Mineral Cycling in Southeastern Ecosystems*, ERDA Symposium Series, CONF-740513. National Information Services, Springfield, VA, pp. 309–313.
- Winker, C.D., Jafe, L.C., Howard, J.D., 1985. *Georgia Estuarine Data, 1961–1977*. Technical Report Series 85-7. Skidaway Institute of Oceanography, Savannah, GA.
- Yassuda, E.A., Davie, S.R., Mendelsohn, D.L., Isaji, T., Peene, S.J., 2000. Development of a waste load allocation model for the Charleston Harbor estuary, phase II: water quality. *Estuarine, Coastal Shelf Sci.* 50, 99–107.
- Zheng, L.Y., Chen, C.S., Liu, H.D., 2003a. A modeling study of the Satilla River Estuary, Georgia. Part I: flooding/drying process and water exchange over the salt marsh-estuary-shelf complex. *Estuaries* 26, 651–669.
- Zheng, L.Y., Chen, C.S., Alber, M., Liu, H.D., 2003b. A modeling study of the Satilla River Estuary, Georgia. Part II: suspended sediment. *Estuaries* 26, 670–679.